

1 **Mitigating the Impact of Increased Drought-Flood 2 Abrupt Alternation Events under Climate Change: The 3 Role of Reservoirs in the Lancang-Mekong River Basin**

4 Keer Zhang¹, Zilong Zhao¹, Fuqiang Tian^{1,2}

5 ¹Department of Hydraulic Engineering & State Key Laboratory of Hydroscience and Engineering,
6 Tsinghua University, 100084, Beijing, China

7 ²Southwest United Graduate School, Kunming 650091, China

8 *Correspondence to:* Fuqiang Tian (tianfq@mail.tsinghua.edu.cn)

9 **Abstract.** The Lancang-Mekong River (LMR) Basin is highly vulnerable to extreme hydrological
10 events, including Drought-Flood Abrupt Alternation (DFAA). The efficacy of potential mitigation
11 measures, such as reservoirs, on DFAA under climate change remains poorly understood. This study
12 investigates these dynamics using five Global Climate Models (GCMs) from the Coupled Model
13 Intercomparison Project Phase 6 (CMIP6). It employs the Revised Short-cycle Drought-Flood Abrupt
14 Alteration Index (R-SDFAI), along with the Tsinghua Representative Elementary Watershed (THREW)
15 model integrated with the developed reservoir module. The findings reveal that DFAA in the LMR
16 Basin is primarily dominated by DTF (drought to flood), with probabilities of DTF exceeding those of
17 FTD (flood to drought) at mild, moderate, and severe intensity levels. The increase in DTF probability
18 for future periods is also significantly higher than that of FTD. Mild DTF and mild FTD account for
19 58% to 90% and 75% to 100% of their total probability in the future, making the mild-intensity events
20 the most frequent DFAA. Reservoirs play a significant role in reducing DTF risks during both dry and
21 wet seasons, though their effectiveness in controlling FTD risks, particularly during the dry season, is
22 relatively weaker. Furthermore, there is a positive correlation between the reservoir's capacity to
23 mitigate total DFAA risk and its total storage. Reservoirs display a stronger ability to regulate
24 high-intensity FTD and high-frequency DTF events, and significantly reduce the monthly duration of
25 DFAA. These insights provide valuable guidance for the effective management of water resources
26 cooperatives across the LMR Basin.

27 **Keywords.** Drought-Flood Abrupt Alternation; Climate change; Reservoir operation; Lancang-Mekong
28 River Basin.

29 **1. Introduction**

30 Flood and drought are two of the most frequent natural disasters in the world (Adikari and Yoshitani,
31 2009; ADREM et al., 2024). Drought-Flood Abrupt Alternation (DFAA), which is defined as the rapid
32 transition between flood and drought conditions within a region (Xiong and Yang, 2025), has received
33 growing attention in recent years (Chen et al., 2025; Wu et al., 2023; Zhang et al., 2012; Shan et al.,
34 2018; Song et al., 2023). DFAA specifically consists of two types of rapid transition events: (1) drought
35 to flood (DTF), where conditions shift quickly from drought to flood, and (2) flood to drought (FTD),
36 where conditions rapidly change from flood to drought. Hazards arising from DFAA are more
37 significant than those from floods and droughts. DFAA not only alters soil conditions and increases the
38 potential for exceeding water quality standards (Bai et al., 2023; Yang et al., 2019) but also challenges
39 food security and seriously affects agricultural production. Furthermore, DFAA, particularly DTF, is
40 prone to triggering severe secondary natural hazards, primarily including flash floods, landslides, and
41 mudslides (Wang et al., 2023).

42 It has been observed that the intensity and frequency of DFAA events demonstrate a global increasing
43 trend (Yang et al., 2022; Chen et al., 2024). However, notable regional differences exist. Shan et al.
44 (2018) observed that the scope of DFAA events in the Yangtze River mid-lower reaches has expanded
45 since the 1960s, with both frequency and intensity increasing annually. Zhang et al. (2012) found that
46 although droughts and floods have increased in the Huai River Basin, DFAA events have become less
47 frequent. Looking ahead, Zhao et al. (2022) projected that the Han River Basin will experience an
48 upward trend in both DFAA frequency and intensity, whereas Yang et al. (2019) reported a projected
49 decline in the frequency of DFAA events in the Hetao region.

50 The Lancang-Mekong River (LMR) Basin, as a significant international river in Southeast Asia,
51 profoundly affects key sectors such as hydropower, agriculture, fisheries, and transport (Morovati et al.,
52 2024). At the same time, the basin is a high-incidence area for floods and droughts (Liu et al., 2020;
53 MRC, 2020). Notably, wet season droughts account for about 40% of annual drought (Tian et al., 2020),
54 while the region is also prone to large floods during the dry season (e.g., May 2006, May 2007,
55 December 2016) (Tellman et al., 2021). The existence of these wet-season droughts and dry-season
56 floods establishes the necessary conditions for DFAA in the LMR Basin.

57 Continued global warming is expected to further intensify both extreme wet and dry climate patterns

58 (IPCC, 2023), contributing to increased vulnerability to DFAA in the future (Yang et al., 2022; Wang et
59 al., 2023; Chen et al., 2025). There is a strong tendency toward more intense floods and droughts in
60 Southeast Asia (IPCC WG1, 2021) and specifically in the LMR Basin (Wang et al., 2021; Li et al.,
61 2021; Dong et al., 2022; Hoang et al., 2016). This heightens concerns about DFAA patterns in the LMR
62 Basin, emphasizing the need for improved water security, sustainable management, and early disaster
63 forecasting and prevention systems.

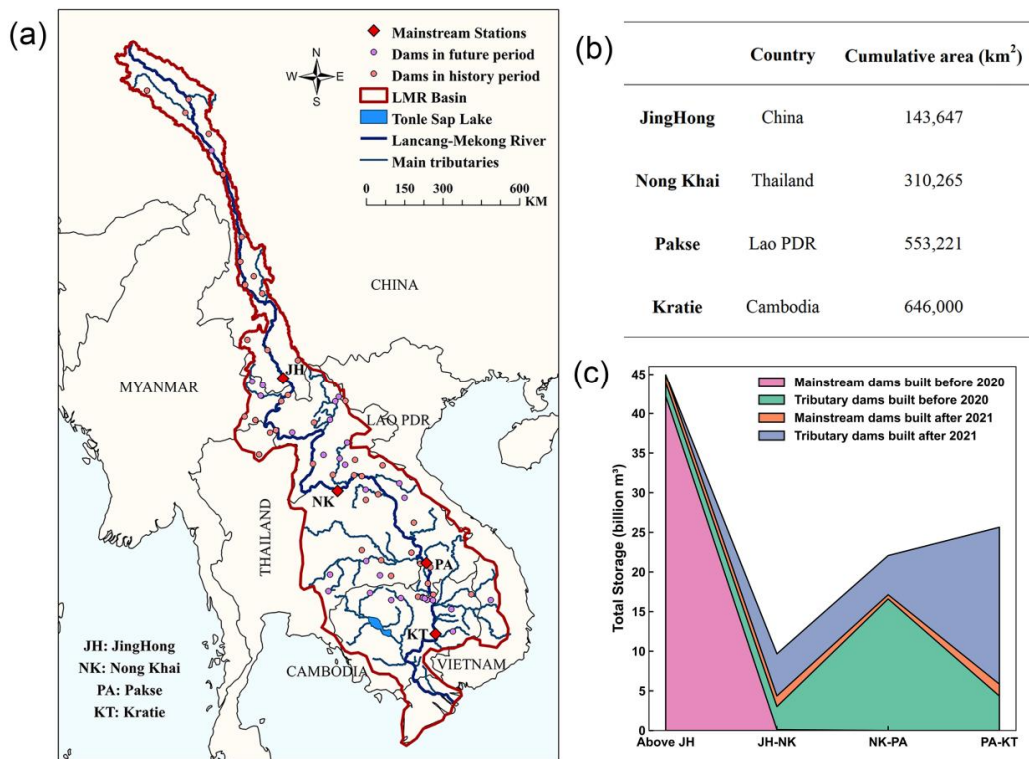
64 The hydrological regime of the LMR Basin is shaped mainly by climate change and human activities
65 (LMC and MRC, 2023). Despite the severe impacts of climate change, human activities such as
66 reservoir operation can help adapt the hydrological regime to these changes (Zhang et al., 2023;
67 Khadka et al., 2023; Sridhar et al., 2019; Lu et al., 2014; Gunawardana et al., 2021). Research
68 highlights that reservoirs play a crucial role in reducing flood damage during the wet season and in
69 minimizing low-flow occurrences (Arias et al., 2014; Räsänen et al., 2012; Dang and Pokhrel, 2024).
70 To evaluate reservoir impacts under the changing climate, integration of a reservoir module within
71 hydrological models is a widely adopted practice. For example, Wang et al. (2017b) demonstrated that
72 reservoir operation can reduce flood intensity and frequency, while Yun et al. (2021a; 2021b) showed
73 that careful reservoir management can relieve both extreme drought and wet events, though with some
74 trade-offs in hydroelectric benefits. Collectively, these studies indicate that reservoirs offer practical
75 adaptation solutions to address climate change impacts.

76 It is essential to consider how human activities, especially reservoir operations, can help manage DFAA
77 under climate change. This consideration supports effective water resource management and the
78 sustainable development of the basin system. However, little research to date has focused on this aspect
79 for the LMR Basin. The statistics, reports, and studies on DFAA in the LMR Basin remain scarce,
80 particularly concerning the mitigating role of reservoirs under the changing climate. In response, this
81 study develops a reservoir module for hydrological modeling, examines the trends of DFAA in the
82 LMR Basin under climate change, and assesses how reservoirs can help basin states adapt to changing
83 conditions. This work aims to advance knowledge on DFAA and support regional water resources
84 management and sustainability.

85 **2. Methodology**

86 **2.1 Study area**

87 The Lancang-Mekong River (LMR) originates from the Tibetan Plateau in China and flows through
 88 China, Myanmar, Laos, Thailand, Cambodia, and Vietnam before entering the South China Sea at the
 89 Mekong Delta. LMR is approximately 4900 km long with a basin area of 812,400 km² (He, 1995). Its
 90 annual runoff is about 475 billion m³ (Sabo et al., 2017; Luo et al., 2023). LMR Basin is characterized
 91 by steep slopes and rapid flows in the upstream. The downstream features shallow slopes and slow,
 92 mixed flows. The wet and dry seasons in the LMR Basin extend from June to November and from
 93 December to May, respectively (LMC and MRC, 2023). These are mainly influenced by the
 94 southwestern and northeastern monsoons. The distribution of the hydrology system and mainstream
 95 hydrological stations in the LMR Basin is detailed in Fig. 1a.



96
 97 **Figure 1: Hydrology of the LMR Basin. (a) Map of rivers and reservoirs, (b) Information on four main**
 98 **hydrological stations, and (c) distribution of reservoir storage. Here, JH, NK, PA, and KT denote JingHong,**
 99 **Nong Khai, Pakse, and Kratie stations, respectively.**

100 LMR Basin nourishes approximately 65 million people. The basin states rely on the river system to
 101 develop economic industries, including capture fisheries, irrigation agriculture, and hydropower. LMR
 102 Basin has the largest freshwater capture fishery in the world (MRC, 2010; MRC, 2019). Its irrigation
 103 area is estimated at around 4.3 million hectares (Do et al., 2020), with the Mekong Delta regarded as

104 Southeast Asia's food basket. LMR Basin is one of the most active regions for hydropower in the world
105 (MRC, 2019; Williams, 2019). It harbors about 235,000 GWhyr⁻¹ of hydroelectric potential in its
106 mainstream and tributaries (Do et al., 2020; Schmitt et al., 2018). LMR Basin is also heavily impacted
107 by floods and droughts. During the past two decades, LMR Basin has experienced several severe
108 droughts (2004-2005, 2009-2010, 2015-2016, and 2019-2020) and floods (Liu et al., 2020; Tian et al.,
109 2020; MRC, 2020). These disasters affect crop cultivation and fisheries harvesting, leading to the loss
110 of property and lives in riparian countries. In 2013 and 2018, floods heavily affected the lower basin,
111 specifically Cambodia, Vietnam, Laos, and Thailand. These floods covered 22.3 and 6.47 thousand km²,
112 respectively (Tellman et al., 2021).

113 **2.2 Data collection**

114 This study utilizes CMIP6 (Sixth Phase of Coupled Model Inter-comparison Project) data as the
115 meteorological input to analyze DFAA. Three SSP (Shared Socioeconomic Pathways) scenarios,
116 namely SSP1-2.6, SSP2-4.5, and SSP5-8.5, are considered to characterize the low-, medium-, and
117 high-emission scenarios, respectively. Five GCMs (Global Climate Models) with wide utilization and
118 proven performance in the LMR Basin are applied in this study (Li et al., 2021; Yun et al., 2021a; Yun
119 et al., 2021b), i.e., GFDL-ESM4, IPSL-CM6A-LR, MPI-ESM1-2-HR, MRI-ESM2-0, and
120 UKESM1-0-LL. The detailed information for these five GCMs is shown in Table 1 (Eyring et al., 2016;
121 Gidden et al., 2019; Cui et al., 2023). CMIP6 data span from 1980 to 2100. This study accordingly
122 considers three research periods: the history period from 1980 to 2014 (consistent with CMIP6), the
123 near future period from 2021 to 2060, and the far future period from 2061 to 2100.

124 In this study, the daily observed runoff data at four major mainstream hydrological stations from 1980
125 to 2020 are used to calibrate and validate the hydrological model. These data are derived from the
126 China Meteorological Administration (CMA) and the Mekong River Commission (MRC). The
127 hydrological stations from upstream to downstream are sequentially JingHong, Nong Khai, Pakse, and
128 Kratie, whose locations and basic information are shown in Figs. 1a and 1b. This study uses the
129 ERA5_Land data as the meteorological input for calibrating and validating the hydrological model, and
130 as the correction dataset for correcting the raw CMIP6 data. ERA5_Land data cover the period from
131 1980 to 2020, with a spatial resolution of 0.1°, and contain precipitation, temperature, and potential
132 evapotranspiration. Soil data are obtained from the Global Soil Database (GSD) provided by the Food

133 and Agriculture Organization of the United Nations (FAO) with a spatial resolution of 10 km x 10 km.
 134 Normalized Vegetation Index (NDVI), Leaf Area Index (LAI), and Snow Cover data are obtained from
 135 MODIS (Moderate-resolution Imaging Spectroradiometer) with a spatial resolution of 500 m x 500 m
 136 and a temporal resolution of 16 days.
 137 Reservoir data are sourced from MRC and Mekong Region Futures Institute (MERFI) (MERFI, 2024).
 138 This study utilizes 122 reservoirs, which simultaneously contain information on location, storage, and
 139 operation years, including 24 reservoirs in the Lancang Basin and 98 reservoirs in the Mekong Basin.
 140 The earliest and latest operation years for them are 1965 and 2035. The location and storage
 141 distribution of these reservoirs are shown in Figs. 1a and 1c.

| Model Name | Modeling Center | Realization | Resolution (Lon×Lat) |
|------------------|--|-------------|-------------------------|
| GFDL-ESM4 | National Oceanic and Atmospheric Administration Geophysical Fluid Dynamics Laboratory, United States | r1i1p1f1 | 1.25°×1° |
| IPSL-CM6A-LR | Institute Pierre Simon Laplace, France | r1i1p1f1 | 2.5°×1.25874° |
| MPI-ESM1-2-HRMax | Planck Institute for Meteorology, Germany | r1i1p1f1 | 0.9375°×0.9375° |
| MRI-ESM2-0 | Meteorological Research Institute, Japan | r1i1p1f1 | 1.125°×1.125° |
| UKESM1-0-LL | Met Office Hadley Centre, UK | r1i1p1f2 | 1.875°×1.25° |

142 **Table 1: Details of 5 GCMs applied in this study.**

143 **2.3 Bias correction method for CMIP6 data**

144 The raw CMIP6 data require correction for more accurate modelling (Hoang et al., 2016; Mishra et al.,
 145 2020; Sun et al., 2023). The uncorrected raw CMIP6 data misestimate the temperature and precipitation
 146 in the LMR Basin, especially overestimating the precipitation (Cui et al., 2023; Lange, 2019; Lange,
 147 2021). ERA5_Land data are used as correction data in this study to address bias in raw CMIP6 data.
 148 This study interpolates the data from the five GCMs of CMIP6, which have different spatial resolutions,
 149 to 0.1° (consistent with ERA5_Land) using the bilinear interpolation spatial resolution method. The
 150 interpolated CMIP6 data are bias-corrected for each GCM according to an N-dimensional probability
 151 density function transform of the multivariate bias correction approach (abbreviated as MBCn)
 152 (Cannon, 2016; Cannon, 2018). The MBCn method is trained based on the difference between
 153 precipitation and temperature data from ERA5_Land and CMIP6 over the history period (1980-2014),
 154 and then applied to the future period (i.e., 2021-2100) to correct the CMIP6 data for each GCM.
 155 The MBCn method considers the multivariate dependency structure of meteorological data and enables
 156 the simultaneous correction of temperature and precipitation data. Random orthogonal rotation and

157 quantile delta mapping are the two most critical formulas of the MBCn method (Cannon, 2018), as
 158 illustrated in Eqs. (1) and (2).

$$159 \quad \begin{cases} \tilde{\mathbf{X}}_T^{[l]} = \mathbf{X}_T^{[l]} \mathbf{R}^{[l]} \\ \tilde{\mathbf{X}}_S^{[l]} = \mathbf{X}_S^{[l]} \mathbf{R}^{[l]} \\ \tilde{\mathbf{X}}_P^{[l]} = \mathbf{X}_P^{[l]} \mathbf{R}^{[l]} \end{cases} \quad (1)$$

160 Eq. (1) displays the process of random orthogonal rotation. It outlines the process of transforming
 161 historical observations $\mathbf{X}_T^{[l]}$, historical climate model simulations $\mathbf{X}_S^{[l]}$, and climate model projections
 162 $\mathbf{X}_P^{[l]}$ using a random orthogonal rotation matrix $\mathbf{R}^{[l]}$ during the l -th iteration. The rotated data are
 163 represented as $\tilde{\mathbf{X}}_T^{[l]}$, $\tilde{\mathbf{X}}_S^{[l]}$, and $\tilde{\mathbf{X}}_P^{[l]}$. This procedure is pivotal for MBCn's multivariate joint distribution
 164 correction, as it transforms the original variable space into new random orientations. In contrast to
 165 conventional univariate correction approaches, MBCn employs a random orthogonal matrix to mix
 166 variables, thereby breaking their independence.

$$167 \quad \begin{cases} \Delta^{(n)[l]}(i) = \tilde{x}_P^{(n)[l]}(i) - F_S^{(n)[l]-1}(F_P^{(n)[l]}(\tilde{x}_P^{(n)[l]}(i))) \\ \hat{x}_P^{(n)[l]}(i) = F_T^{(n)[l]-1}(F_P^{(n)[l]}(\tilde{x}_P^{(n)[l]}(i))) + \Delta^{(n)[l]}(i) \end{cases} \quad (2)$$

168 Eq. (2) exhibits the quantile delta mapping, which defines how quantile delta mapping is applied to the
 169 n -th dimension of the rotated climate model projection data $\tilde{x}_P^{(n)[l]}(i)$ within the rotated space of the
 170 l -th iteration. Here, $\Delta^{(n)[l]}(i)$ represents the quantile difference between the historical climate model
 171 simulations and climate model projections in the l -th iteration and the n -th dimension. $F_P^{(n)[l]}$ denotes
 172 the empirical cumulative distribution function for the rotated climate model projection data in the n -th
 173 dimension. $F_T^{(n)[l]-1}$ and $F_S^{(n)[l]-1}$ denote inverse Functions of the empirical cumulative distribution
 174 functions for the rotated historical observation data and historical climate model simulation data in the
 175 n -th dimension. This step preserves the trend of the climate model projection data throughout the
 176 correction process. The number of iterations is typically set to 10-30.

177 The MBCn algorithm performs multivariate joint distribution bias correction by iteratively applying
 178 random orthogonal rotation and quantile delta mapping, while preserving the projected signals in the
 179 climate model. The rotation operation breaks dependencies between variables, enabling the quantile
 180 delta mapping of a single variable to indirectly adjust multivariate correlations. The quantile delta
 181 mapping ensures the transmission of absolute or relative trends by computing quantile differences
 182 between the historical and projected periods of the climate model. The MBCn method has been

183 reported to increase correction precision and accuracy compared to univariate and other multivariate
184 bias correction algorithms (Cannon, 2018).

185 In addition, this study utilized the method proposed by Van Pelt et al. (2009) to compute daily potential
186 evapotranspiration data for five GCMs under three SSP scenarios, based on daily temperature. The
187 computational approach is outlined in Eq. (3).

188
$$PET = [1 + \alpha_0(T - \bar{T}_0)]\bar{PET}_0 \quad (3)$$

189 Where, \bar{T}_0 and \bar{PET}_0 correspond to the daily air temperature ($^{\circ}\text{C}$) and daily potential
190 evapotranspiration (mm day^{-1}) in the history period sourced from ERA5_Land datasets. T signifies
191 the corrected daily air temperature ($^{\circ}\text{C}$) from CMIP6 datasets. The parameter α_0 is determined by the
192 relationship between daily potential evapotranspiration and daily temperature in ERA5_Land data
193 during the history period.

194 **2.4 Hydrological model coupled with reservoir module**

195 The THREW (Tsinghua Representative Elementary Watershed) hydrological model is applied in this
196 study for runoff simulation. It utilizes the Representative Elementary Watershed (REW) approach for
197 spatial division, and further subdivides the REW into eight distinct hydrological zones: vegetated zone,
198 bare soil zone, glacier covered zone, snow covered zone, sub-stream-network zone, main channel reach,
199 saturated zone, and unsaturated zone (Tian et al., 2006; Mou et al., 2008).

200 The model is built upon scale-coordinated equilibrium equations, geometrical relationships, and
201 constitutive relationships, and enables comprehensive simulation of complex hydrological processes
202 from mountain to ocean. The fundamental balance equations in the THREW model are listed in Eqs. (4)
203 to (6).

204
$$\frac{d}{dt}(\bar{\rho}_\alpha^j \epsilon_\alpha^j y^j \omega^j) = \sum_p e_\alpha^{jP} + \sum_{\beta \neq \alpha} e_{\alpha\beta}^j \quad (4)$$

205 Eq. (4) demonstrates the general form of the mass conservation equation at the REW scale. $\frac{d}{dt}$ denotes
206 the time derivative. $\bar{\rho}_\alpha^j$ refers to the time-averaged density of phase α in sub-region j , in $\text{kg}\cdot\text{m}^{-3}$. ϵ_α^j
207 means the volume fraction of phase α within sub-region j . y^j indicates the time-averaged thickness of
208 sub-region j , in m. ω^j means the time-averaged fraction of REW horizontal area occupied by
209 sub-region j . e_α^{jP} denotes the net mass exchange flux of phase α in sub-region j through interface P
210 (e.g., with atmosphere, groundwater, neighboring REWs), in $\text{kg}\cdot\text{m}^{-2}\cdot\text{s}^{-1}$, where a positive value

211 indicates the inflow to sub-region j . $e_{\alpha\beta}^j$ refers to the phase transition rate between phase α and phase
 212 β within sub-region j , in $\text{kg}\cdot\text{m}^{-2}\cdot\text{s}^{-1}$, where a positive value indicates phase α gains mass from phase
 213 β . Sub-region here refers to the eight zones within each REW.

$$214 (\overline{\rho_\alpha^j} \overline{\epsilon_\alpha^j} \overline{y^j} \overline{\omega^j}) \frac{d\overline{v_\alpha^j}}{dt} = \overline{g_\alpha^j} \overline{\rho_\alpha^j} \overline{\epsilon_\alpha^j} \overline{y^j} \overline{\omega^j} + \sum_P T_\alpha^{jP} + \sum_{\beta \neq \alpha} T_{\alpha\beta}^j \quad (5)$$

215 Eq. (5) presents the general form of the momentum conservation equation at the REW scale. $\overline{v_\alpha^j}$
 216 indicates the time-averaged velocity vector of phase α in sub-region j , in $\text{m}\cdot\text{s}^{-1}$. $\overline{g_\alpha^j}$ denotes the
 217 time-averaged gravity vector of phase α in sub-region j , in $\text{m}\cdot\text{s}^{-2}$. T_α^{jP} means the force vector
 218 (pressure, friction, seepage) exerted on phase α in sub-region j by interface P , in $\text{N}\cdot\text{s}^{-2}$, representing
 219 the momentum exchange. $T_{\alpha\beta}^j$ refers to the interfacial force vector between phase α and phase β
 220 within sub-region j , in $\text{N}\cdot\text{s}^{-2}$, including drag and capillarity.

$$221 (\overline{\epsilon_\alpha^j} \overline{y^j} \overline{\omega^j} \overline{c_\alpha^j}) \frac{d\overline{\theta_\alpha^j}}{dt} = \overline{h_\alpha^j} \overline{\rho_\alpha^j} \overline{\epsilon_\alpha^j} \overline{y^j} \overline{\omega^j} + \sum_P Q_\alpha^{jP} + \sum_{\beta \neq \alpha} Q_{\alpha\beta}^j \quad (6)$$

222 Eq. (6) exhibits the general form of the heat conservation equation at the REW scale. c_α^j means the
 223 specific heat capacity (constant volume) of phase α in sub-region j , in $\text{J}\cdot\text{kg}^{-1}\cdot\text{K}^{-1}$. $\overline{\theta_\alpha^j}$ refers to the
 224 time-averaged temperature of phase α in sub-region j , in K . $\overline{h_\alpha^j}$ denotes the heat generation rate per
 225 unit mass within phase α in sub-region j , in $\text{W}\cdot\text{kg}^{-1}$ (e.g., radioactive decay, negligible usually). Q_α^{jP}
 226 indicates the heat exchange rate between phase α in sub-region j and its environment via interface P ,
 227 in $\text{W}\cdot\text{m}^{-2}$, with the positive value representing the heat gained by phase α in sub-basin j . $Q_{\alpha\beta}^j$ refers
 228 to the heat exchange rate between phase α and phase β within sub-region j , in $\text{W}\cdot\text{m}^{-2}$, with a positive
 229 value indicating that heat is gained by phase α .

230 The THREW model employs an automatic calibration procedure to calibrate hydrological parameters
 231 through parallel computation (Nan et al., 2021). The calibration period of the THREW model in the
 232 LMR Basin is from 2000 to 2009, and the validation period is from 2010 to 2020. The Nash-Sutcliffe
 233 efficiency coefficient (NSE) indicator is adopted to calibrate the objective function and evaluate
 234 simulation effectiveness at the daily scale, which is calculated according to Eq. (7). The THREW
 235 model has been successfully applied to a number of basins with various climate characteristics
 236 worldwide (Tian et al., 2012; Lu et al., 2021; Morovati et al., 2023; Cui et al., 2023; Zhang et al.,
 237 2023).

238
$$NSE = 1 - \frac{\sum_{num=1}^N (Q_{obs}^{num} - Q_{sim}^{num})^2}{\sum_{num=1}^N (Q_{obs}^{num} - \bar{Q}_{obs})^2} \quad (7)$$

239 Where, Q_{obs}^{num} is the daily observed runoff, Q_{sim}^{num} is the daily simulated runoff, \bar{Q}_{obs} is the average of
240 observed runoff, and N is the total number of days.

241 This study extends the THREW model by developing and integrating a reservoir management module.
242 This integration allows the expanded THREW model to use detailed data on 122 reservoirs in the LMR
243 Basin, with operational years ranging from 1965 to 2035. By specifying whether the module is active,
244 the model can simulate either natural runoff (without considering reservoirs) or dammed runoff (with
245 reservoirs included). This setup ensures a seamless interaction between the core model and the
246 reservoir operations framework.

247 Reservoir operation follows consistent rules across time and space, with each reservoir starting
248 operation according to its operational year. Strategies are adapted in response to inflow fluctuations and
249 administered on a daily scale. Each reservoir is assigned based on location. Cumulative multi-year
250 sub-basin storage is calculated as input for the reservoir module, which operates in two phases: initial
251 and normal. The normal phase is divided into general and emergency cases, both using the same
252 operation rules but differing constraints; the emergency case allows more flexibility. The module's
253 flowchart is illustrated in Fig.2.

254 If a REW's cumulative multi-year storage changes within a year, it signals the start of a new reservoir's
255 operation, which follows initial phase rules. During the initial phase, the outlet flow matches the inlet if
256 it is below the minimum discharge constraint; otherwise, it meets the minimum discharge constraint.
257 The rules for the initial phase are described as Eqs. (8) to (9). Storage and discharge constraints are
258 defined in Eqs. (10) to (11) (Tennant, 1976; Yun et al., 2020). The initial phase ends when reservoir
259 storage exceeds the minimum constraint (Eq. (12)), then transitions to the normal phase.

260
$$Q_{out} = \begin{cases} Q_{in}, & Q_{in} < Q_{min} \\ Q_{min}, & Q_{in} \geq Q_{min} \end{cases} \quad (8)$$

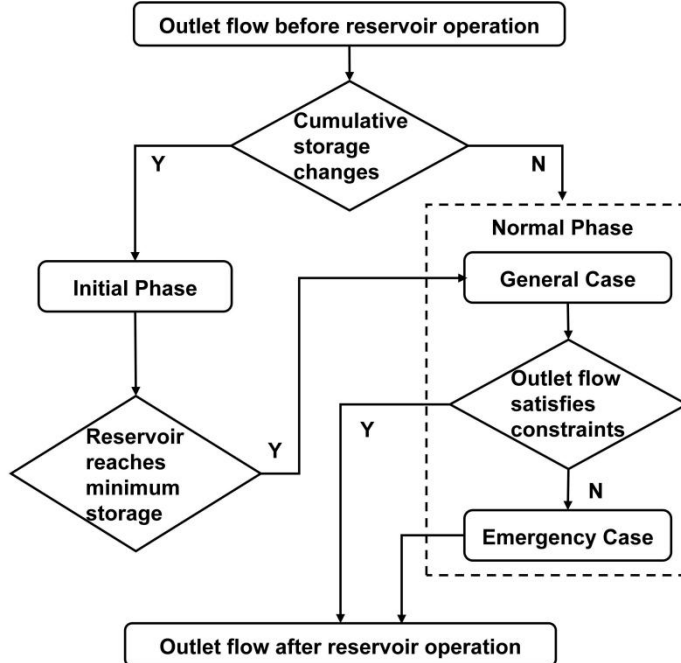
261
$$S_t = S_{t-1} + Q_{in} - Q_{out} \quad (9)$$

262
$$S_{min} = 0.2 \times S_{total} \quad (10)$$

263
$$Q_{min} = 0.6 \times Q_{ave} \quad (11)$$

264
$$S_t \geq S_{min} \quad (12)$$

265 Where Q_{out} is the outlet flow, Q_{in} is the inlet flow, Q_{min} is the minimum discharge constraint, S_t is
 266 the storage for time t , S_{min} is the minimum storage constraint, S_{total} is the total storage, and Q_{ave} is
 267 the average multi-year runoff during the calibration period (i.e., 2000-2009).



268

269 **Figure 2: Flowchart of the constructed reservoir module.**

270 The scheduling rule for the normal phase is the improved Standard Operation Policy hedging model
 271 (SOP) (Wang et al., 2017a; Morris and Fan, 1998), as depicted in Eq. (9) and Eqs. (13) to (16). Under
 272 the premise of water balance (Eq. (9)), constraints for annual storage (Eq. (13)), outlet flow (Eq. (14)),
 273 wet season storage (Eq. (15)), and dry season storage (Eq. (16)) are considered separately, where
 274 priority is given to the annual storage constraint (Eq. (13)).

275 $S_{min} \leq S_t \leq S_{max}$ (13)

276 $Q_{min} \leq Q_{out} \leq Q_{max}$ (14)

277 $\min|S_c - S_t|, \text{month} = 6,7,8,9,10,11$ (15)

278 $\min|S_n - S_t|, \text{month} = 12,1,2,3,4,5$ (16)

279 Where Q_{max} is the maximum discharge constraint, S_{max} is the maximum storage constraint, S_c is
 280 the storage corresponding to the flood control level, and S_n is the storage corresponding to the normal
 281 water level.

282 When in the normal phase, the reservoir first applies general case constraints (Eqs. (17) to (22)). If
283 outlet flow is not fully satisfied (Eq. (14)), constraints switch to the emergency case, and the reservoir
284 is rescheduled. Eq. (23) signals an emergency case start, which provides more flexible flow limits to
285 avoid extremes. Emergency case constraints are in Eqs. (24) to (25).

286 $Q_{max} = 2 \times Q_{ave}$ (17)

287 $Q_{min} = 0.6 \times Q_{ave}$ (18)

288 $S_c = S_{min} \times 1.2$ (19)

289 $S_n = S_{max} \times 0.8$ (20)

290 $S_{min} = 0.2 \times S_{total}$ (21)

291 $S_{max} = \begin{cases} 0.8 \times S_{total}, & month = 6,7,8,9,10,11 \\ 1 \times S_{total}, & month = 12,1,2,3,4,5 \end{cases}$ (22)

292 $Q_{min} \leq Q_{out}' \leq Q_{max}$ (23)

293 $Q_{min} = 0.3 \times Q_{ave}$ (24)

294 $S_{max} = 0.8 \times S_{total}$ (25)

295 Where Q_{out}' is the outlet flow after the scheduling in the general case.

296 **2.5 Indicator for DFAA**

297 It is common practice to quantify DFAA incidents via indices. LDFAI, proposed by Wu et al. (2006),
298 quantitatively characterizes long-term DFAA during the wet season and has been widely adopted (Ren
299 et al., 2023; Shi et al., 2021; Yang et al., 2022; Yang et al., 2019). Building on this, Zhang et al. (2012)
300 introduced the one-month interval SDFAI, extending its application from precipitation to runoff and
301 characterizing short-term DFAA. SDFAI has since been applied in fields such as hydrology,
302 meteorology, ecology, and agriculture (Zhao et al., 2022; Lei et al., 2022; Yang et al., 2019; Zhang et al.,
303 2019).

304 Song et al. (2023) proposed the Revised Short-cycle Drought-Flood Abrupt Alteration Index
305 (R-SDFAI), which extends the LDFAI and SDFAI time frame from only the flood season to the entire
306 year, facilitating multi-year DFAA analysis. R-SDFAI also addresses issues of over-identification,
307 under-identification, and misrepresentation of DFAA severity found in SDFAI. Therefore, this study

308 uses R-SDFAI for DFAA analysis, with the formulas outlined in Eqs. (26) to (31) (Song et al., 2023).

309 $F_1 = S_{i+1} - S_i$ (26)

310 $F_2 = |S_{i+1}| + |S_i|$ (27)

311 $F = \left| \frac{F_1}{F_2} \right|^{S_{i+1} + S_i}$ (28)

312 $I = F \times \min(|S_{i+1}|, |S_i|)$ (29)

313 $I' = \left(\frac{I}{0.5} \right)^{\frac{\max(|S_{i+1}|, |S_i|)^2}{|F_1| + F_2}} \times \frac{\frac{\max(|S_{i+1}|, |S_i|)}{|F_1| + F_2} + \frac{\min(|S_{i+1}|, |S_i|)}{|F_1| + F_2}}{2}$ (30)

314 $R - SDFAI = sign(F_1) \times \left(\frac{I'}{I_{0.5}} \times \frac{I}{0.5} \right)^{\left[\frac{\max(|S_{i+1}|, |S_i|)}{|F_1| + F_2} \right]^{1 - \frac{\max(|S_{i+1}|, |S_i|)}{|F_1| + F_2}}}$ (31)

315 Where, S_i refers to the SRI in month i, F_1 denotes the intensity of DFAA, F_2 denotes the absolute
316 intensity of drought and flood, and F is a weighting factor between 0 and 1. $I'_{0.5}$ refers to I' when
317 $I=0.5$.

318 The calculation process of SRI utilized in this work is explained in Eqs. (32) to (37). Eq. (32) gives the
319 probability density function that satisfies the Gamma distribution for runoff x at a given time period.

320 $g(x) = \frac{1}{\beta^\alpha \Gamma(\alpha)} x^{\alpha-1} e^{-\frac{x}{\beta}}, x > 0$ (32)

321 Where, $\alpha > 0$ and $\beta > 0$ are respectively the shape and scale parameters. $\hat{\alpha}$ and $\hat{\beta}$ are the optimal
322 values of α and β , obtained according to the maximum likelihood estimation method, as illustrated in
323 Eqs. (33) to (35). $\Gamma(\alpha)$ is the gamma function, as given in Eq. (36).

324 $\hat{\alpha} = \frac{1}{4A} (1 + \sqrt{1 + \frac{4A}{3}})$ (33)

325 $\hat{\beta} = \frac{\bar{x}}{\hat{\alpha}}$ (34)

326 $A = \ln(\bar{x}) - \frac{\sum \ln(x_i)}{num}$ (35)

327 $\Gamma(\alpha) = \int_0^\infty y^{\alpha-1} e^{-y} dy$ (36)

328 Where, x_i is the sample of runoff sequence, \bar{x} is the average runoff, and num is the length of the
329 runoff sequence.

330 Then the cumulative probability of runoff x is illustrated in Eq. (37).

331
$$G(x) = \int_0^x g(x) dx = \frac{1}{\beta^{\hat{\alpha}} \Gamma(\hat{\alpha})} \int_0^x x^{\hat{\alpha}-1} e^{-\frac{x}{\beta}} dx, \quad x > 0 \quad (37)$$

332 The R-SDFAI index identifies DFAA events with a threshold of ± 1 (Song et al., 2023), and further
 333 categorizes DFAA events into three intensity levels—mild, moderate, and severe—using thresholds of
 334 ± 1 , ± 1.44 , and ± 1.88 , as demonstrated in Table 2. This classification follows the criteria proposed by
 335 Song et al. (2023). The underlying rationale involves using ± 0.5 , ± 1 , and ± 1.5 as thresholds for the
 336 SRI index to categorize extreme hydrological events into mild, moderate, and severe droughts and
 337 floods (positive values indicate flood, while negative values indicate drought). The R-SDFAI index
 338 values of ± 1 , ± 1.44 , and ± 1.88 are calculated through the transitions between mild drought and mild
 339 flood, moderate drought and moderate flood, and severe drought and severe flood. These thresholds
 340 serve as the classification criteria for mild, moderate, and severe DFAA events. For a more detailed
 341 explanation of this classification standard, please refer to Song et al. (2023). In this study, the
 342 frequency of DFAA events is represented by their occurrence probabilities during history, near future,
 343 and far future periods, while the intensity of DFAA is assessed through the probability of different
 344 intensity events.

| Event | Intensity | Classification |
|-------|-----------|-------------------------------------|
| DTF | Mild | $1 \leq R\text{-SDFAI} < 1.44$ |
| | Moderate | $1.44 \leq R\text{-SDFAI} < 1.88$ |
| | Severe | $R\text{-SDFAI} \geq 1.88$ |
| FTD | Mild | $-1.44 < R\text{-SDFAI} \leq -1$ |
| | Moderate | $-1.88 < R\text{-SDFAI} \leq -1.44$ |
| | Severe | $R\text{-SDFAI} \leq -1.88$ |

345 **Table 2: The evaluation criteria and intensity classification for DFAA events.**

346 **2.6 Scenario Setting**

347 This study examines two scenarios: dammed (with reservoir operations) and natural (without reservoir
 348 operations). Meteorological data from five GCMs under three SSPs are downscaled to the REW scale
 349 and used as input for the THREW model. The model, with the reservoir module, simulates runoff at
 350 key hydrological stations for the history period (1980-2014), the near future (2021-2060), and the far
 351 future (2061-2100). Both scenarios—with and without reservoir management—are examined. The
 352 R-SDFAI indicator evaluates DFAA event probabilities for each period and each scenario, using runoff
 353 simulated by the 5 GCMs and 3 SSPs.

354 This study adopts the difference in DFAA's probability between the natural scenario (without reservoir
355 operations) and the dammed scenario (with reservoir operations) to capture the reservoir's impact, as
356 shown in Eq. (38).

357 $P_{Impact\ of\ Reservoirs,i,e} = P_{Dammed,i,e} - P_{Natural,i,e}$ (38)

358 Where $P_{Impact\ of\ Reservoirs,i,e}$ represents the impact of reservoirs on the probability of event e in period
359 i . $P_{Natural,i,e}$ denotes the probability of event e under the natural scenario in period i , while $P_{Dammed,i,e}$
360 denotes the probability of event e under the dammed scenario in period i . Period i refers to the near
361 future and far future periods. Event e indicates the DTF, FTD, and DFAA events.
362 Eqs. (39) and (40) give the definitions of $P_{Natural,i,e}$ and $P_{Dammed,i,e}$ described above.

363 $P_{Natural,i,e} = \frac{M_{Natural,i,e}}{TM_i}$ (39)

364 $P_{Dammed,i,e} = \frac{M_{Dammed,i,e}}{TM_i}$ (40)

365 Where $M_{Natural,i,e}$ denotes the number of months in which event e occurs in period i under the natural
366 scenario. $M_{Dammed,i,e}$ denotes the number of months occurred event e in period i under the dammed
367 scenario. TM_i refers to the total number of months in period i . Period i refers to the near future and far
368 future periods. Event e indicates the DTF, FTD, and DFAA events.

369 As each GCM possesses a unique structure and assumptions, projections of climate change by a single
370 GCM inherently possess uncertainties, which in turn introduce uncertainties in the simulation of
371 hydrological outcomes (Kingston et al., 2011; Thompson et al., 2014). Thus, averaging across multiple
372 GCMs is a crucial approach, as it minimizes model biases, eliminates outliers, reduces uncertainties,
373 and ensures more robust and universally applicable outcomes (Lauri et al., 2012; Hoang et al., 2016;
374 Hecht et al., 2019; Wang et al., 2024; Yun et al., 2021b). This method has been extensively employed in
375 prior studies (Dong et al., 2022; Li et al., 2021; Wang et al., 2022; Yun et al., 2021a). Therefore, this
376 research determines the average DFAA probability from five GCMs to lessen the uncertainty in their
377 predictions and assesses the fluctuation in these probabilities across the models to demonstrate their
378 variability.

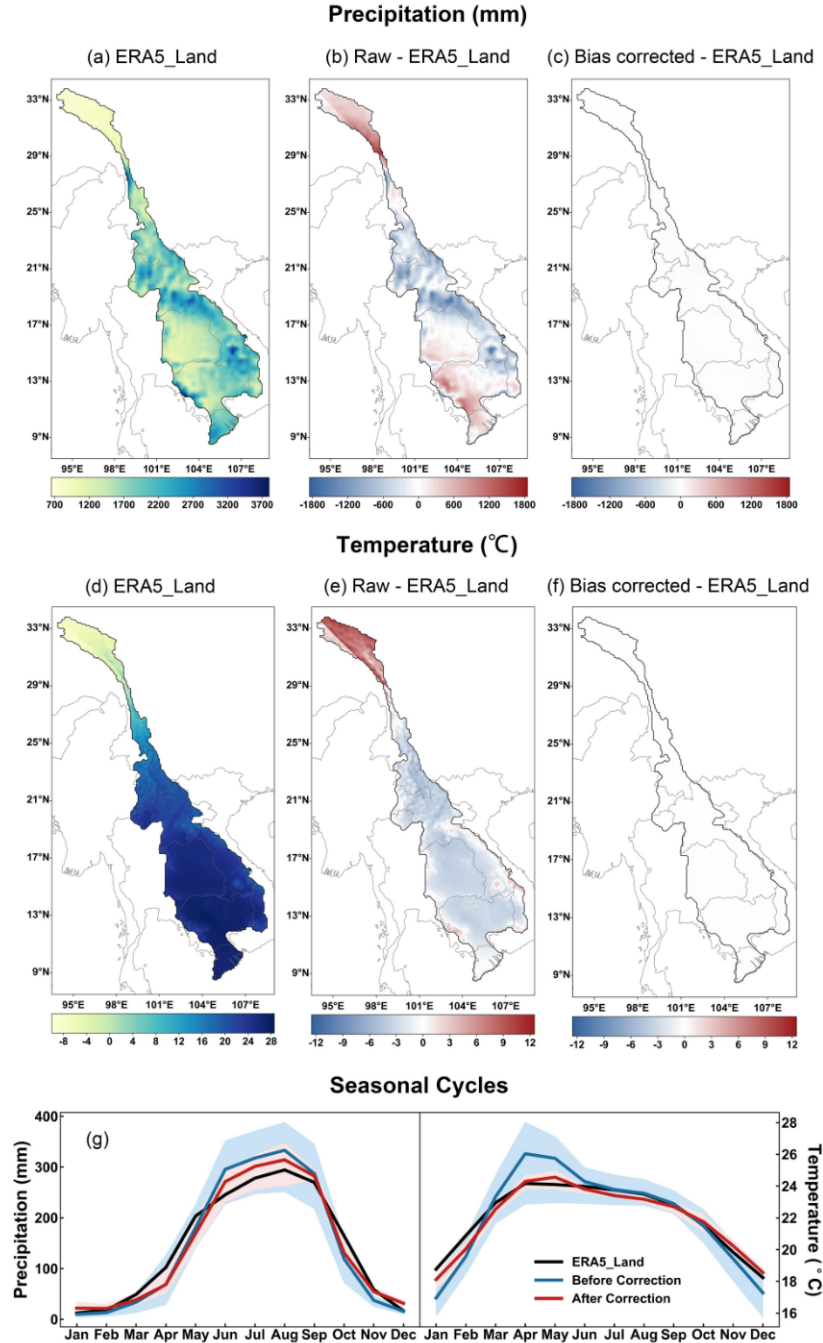
379 **3. Result**

380 **3.1 CMIP6 data bias correction performance**

381 From both regional and seasonal perspectives, the uncorrected raw CMIP6 data show significant
382 discrepancies with ERA5_Land data during the history period (1980-2014). When compared with
383 ERA5_Land data, the uncorrected raw CMIP6 data reveal an average annual precipitation bias of
384 ± 1800 mm and an average daily temperature of ± 12 °C (Figs. 3b and 3e). These notable
385 inconsistencies highlight that using uncorrected CMIP6 data for hydrological modeling would incur
386 considerable inaccuracies. However, CMIP6 data corrected by the MBCn method deviate from
387 ERA5_Land data by no more than ± 120 mm of average annual precipitation and ± 0.2 °C of average
388 daily temperature (Figs. 3c and 3f). The bias correction greatly improves CMIP6 data accuracy in the
389 LMR Basin. The corrected CMIP6 data also match the seasonal cycle of ERA5_Land well for both
390 precipitation and temperature (Fig. 3g). Compared to the raw data, the corrected CMIP6 shows much
391 improved spatial and temporal accuracy, leading to more accurate and reasonable analyses for DFAA.

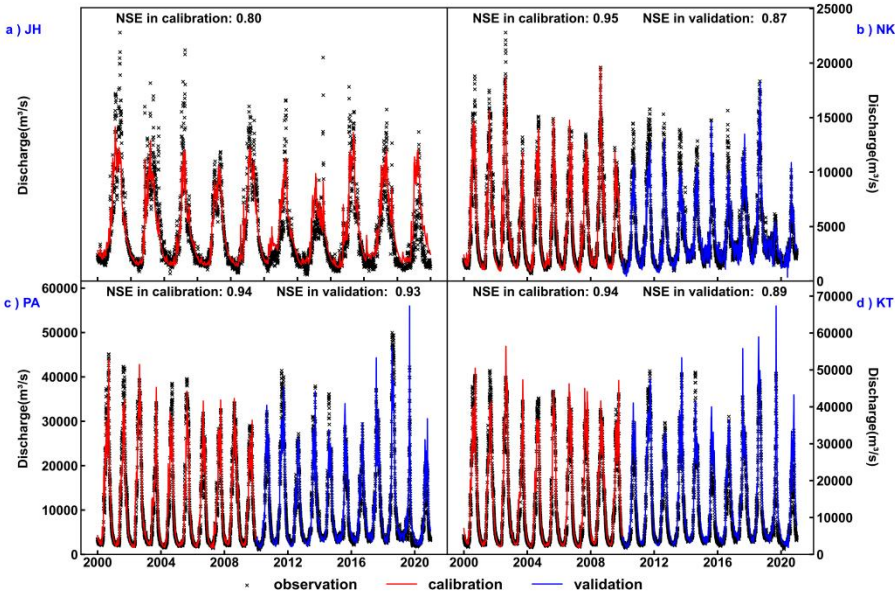
392 **3.2 Calibration and validation for the hydrological model**

393 The daily observed runoff and daily simulated runoff from the THREW model for the calibration
394 period (2000-2009) and validation period (2010-2020) are illustrated in Fig. 4, demonstrating the
395 model's strong performance. Importantly, since there was no massive reservoir construction in the
396 LMR Basin before and during the calibration period (Zhang et al., 2023), the THREW model without
397 the reservoir module is applied for calibration. Meanwhile, the addition of large-scale reservoirs during
398 the validation period allows validation of the THREW model configuration with the reservoir module,
399 Notably, the THREW model captures runoff fluctuations between wet and dry seasons with high
400 accuracy, achieving an NSE of at least 0.8 during both periods. This excellent simulation performance
401 extends across both upstream and downstream regions, emphasizing the robustness of the model under
402 observed conditions.



403

404 Figure 3: Averaged meteorological data of 5 GCMs for the history period (1980-2014). Here, 5 GCMs are
 405 corrected separately. (a)-(c) present the spatial distribution of precipitation based on respectively
 406 ERA5_Land, raw CMIP6 (raw CMIP6 minus ERA5_Land) and bias-corrected CMIP6 (bias-corrected
 407 CMIP6 minus ERA5_Land). (d)-(f) illustrate the spatial distribution of temperature based on ERA5_Land,
 408 raw CMIP6 (raw CMIP6 minus ERA5_Land) and bias-corrected CMIP6 (bias-corrected CMIP6 minus
 409 ERA5_Land). (g) seasonal cycles of temperature and precipitation from ERA5_Land, raw and
 410 bias-corrected CMIP6, as well as their corresponding range.



411

412 **Figure 4: Performance of the THREW model in calibration (2000-2009) and validation (2010-2020) periods.**

413 Here, JH, NK, PA, and KT denote JingHong, Nong Khai, Pakse, and Kratie stations, respectively.

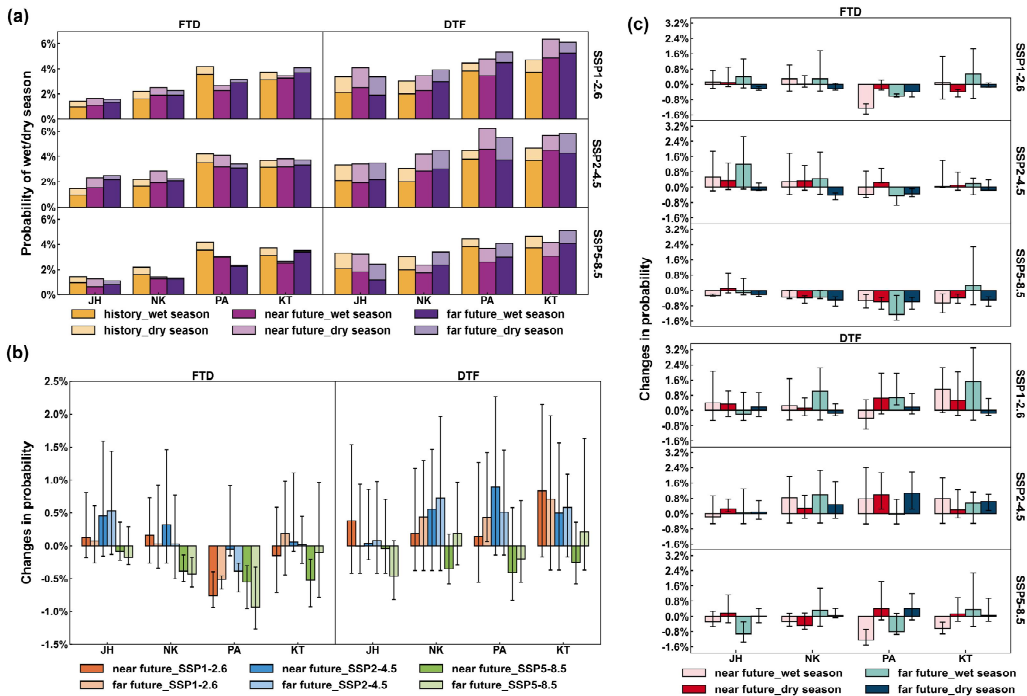
414 **3.3 DFAA under the changing climate**

415 Under the natural scenario (without reservoir operations), DFAA in the LMR Basin is dominated by
 416 DTF, that is, the risk of DTF is more critical than that of FTD (Fig. 5a). The probability of FTD ranges
 417 from 0.7% to 2.1% in the history period, 0.6% to 2.0% in the near future, and 0.5% to 2.0% in the far
 418 future. Conversely, DTF probabilities are higher, ranging from 1.6% to 2.3%, 1.2% to 3.2%, and 1.2%
 419 to 3.0% respectively in these three periods.

420 DFAA risk is substantially elevated during the wet season compared to the dry season (Fig. 5a). For the
 421 average of five GCMs, the probability of FTD in the wet season is 2 to 5.5 times higher than that in the
 422 dry season in the history period. In the near and far future periods, this ratio ranges from 1.1 to 36 times
 423 and 3.3 to 41 times, respectively. As for DTF, the probability in the wet season is correspondingly 1.7
 424 to 5.7 times, 1.3 to 3.9 times, and 0.9 to 6.3 times higher than that in the dry season for history, near
 425 future, and far future. Only JingHong station experiences a slightly higher probability of DTF in the
 426 dry season (1.25%) than in the wet season (1.17%) for the far future.

427 DFAA risks show marked spatial variation, with annual probability consistently higher downstream
 428 than upstream (Fig. 5a). The annual probability of FTD ranges from 0.6% to 1.3% at JingHong station
 429 and 0.7% to 1.4% at Nong Khai station. These probabilities rise to 1.2% to 2.1% and 1.4% to 2.1% at
 430 Pakse and Kratie stations, respectively. Similarly, the annual probability of DTF at JingHong and Nong
 431 Khai stations is 1.2% to 2.1% and 1.2% to 2.3%. The probabilities at Pakse and Kratie stations range

432 from 1.4% to 3.2% and 3.1% to 3.2%, respectively. The DTF risk in the wet season and the FTD risk in
 433 both dry and wet seasons are also higher downstream than upstream. Since the probability of FTD in
 434 the dry season at Nong Khai, Pakse, and Kratie stations is limited, especially under the SSP5-8.5
 435 scenario (<0.2%), the risk of FTD in the dry season appears more notable upstream than downstream.



436
 437 **Figure 5: DFAA under the natural scenario. Here, JH, NK, PA, and KT respectively denote JingHong,**
 438 **Nong Khai, Pakse, and Kratie stations. (a) Seasonal probability of DFAA averaged across five GCMs**
 439 **during the history (1980-2014), near future (2021-2060), and far future (2061-2100) periods, as well as under**
 440 **three SSPs. The annual probability is half of the sum of wet and dry season probabilities. (b) The annual**
 441 **change in DFAA probability averaged across five GCMs and their ranges in the near and far future periods**
 442 **with respect to the history period under three SSPs. (c) The seasonal change in DFAA probability averaged**
 443 **across five GCMs and their ranges in the near and far future periods with respect to the history period**
 444 **during wet and dry seasons under three SSPs.**

445 The annual DFAA probability increases under SSP1-2.6 and SSP2-4.5 scenarios (except for FTD at
 446 Pakse station) and decreases under the SSP5-8.5 scenario (Fig. 5b). Such a pattern is attributable to the
 447 enhanced tendency for flood and drought events in the LMR Basin to cluster rather than alternate under
 448 the SSP5-8.5 scenario (Dong et al., 2022). Under SSP5-8.5 scenario, the average probability of FTD
 449 across five GCMs is 0.6% to 1.8%, while the probability of DTF ranges from 1.2% to 2.6%.
 450 Conversely, the average probabilities of FTD and DTF under the SSP2-4.5 scenario range from 0.7% to
 451 2.1% and 1.7% to 3.2%, respectively.

452

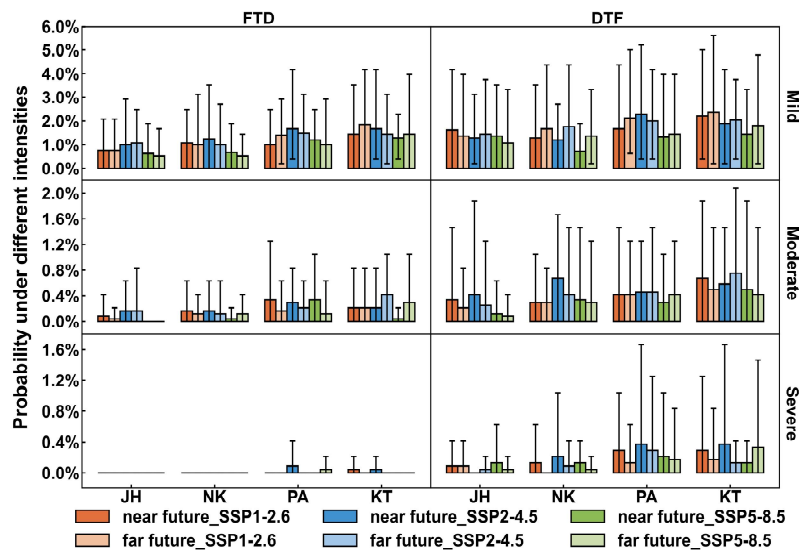
453 The future growth in DTF is significantly greater than that in FTD. For the average probabilities across
454 five GCMs, relative to the history period, the future change in DTF probability at JingHong station is
455 -0.5% to 0.4%, at Nong Khai station is -0.4% to 0.7%, and at Pakse and Kratie stations, respectively, is
456 -0.5% to 0.9% and -0.2% to 0.8%. The future FTD probability change for JingHong is -0.2% to 0.5%,
457 while for Nong Khai, Pakse, and Kratie, it is -0.4% to 0.3%, -1% to -0.1%, and -0.6% to 0.2%,
458 respectively. The maximum values from the five GCMs show a consistent trend, with increases in DTF
459 probability being significantly greater than those in FTD probability.

460 Upstream and downstream regions experience contrasting future risk increases, with FTD risks rising
461 more upstream and DTF risks rising more downstream (Fig. 5b). Under three climate models, Jinghong
462 Station experiences the maximum increase of 0.37% and 0.08% in DTF risks, respectively, in the near
463 and far future. Meanwhile, FTD risks at this station rise by 0.45% and 0.53%, respectively. Conversely,
464 Kratie Station exhibits the highest increase of 0.83% and 0.71% in DTF risks, alongside 0.06% and
465 0.02% increases in FTD risks. The opposite trends of DFAA risk in upstream and downstream pose
466 enhanced challenges to the integrated management of the LMR Basin.

467 Future seasonal DFAA risks follow scenario-dependent trends: wet-season risks for both DTF and FTD
468 rise under SSP1-2.6 and SSP2-4.5 scenarios, and fall under the SSP5-8.5 scenario (Fig. 5c). This is
469 similar to the annual DFAA risk. The risk of FTD during the dry season decreases, with an upward
470 trend emerging only in the near future under the SSP2-4.5 scenario (average across five GCMs <0.4%,
471 maximum <1.3%). The risk of DTF during the dry season rises in most situations, except at Nong Khai
472 station in the near future under the SSP5-8.5 scenario, where it shows an average decrease of 0.46%
473 across five GCMs. The largest increase of dry-season risk of DTF is found at Pakse station under the
474 SSP2-4.5 scenario, with an average increase of 1.08% across five GCMs and a maximum increase of
475 2.08%.

476 Mild-intensity DFAA events constitute the majority of all DFAA occurrences (Fig. 6). The probability
477 of mild DTF varies across scenarios, with values ranging from 0.7% to 2.4%, which corresponds to
478 58% to 90% of the total DTF probability. Likewise, mild FTD probabilities range from 0.6% to 1.8%
479 (Fig. 6), comprising a larger share of the total FTD probability, specifically 75% to 100%. Mild DTF
480 events account for 2 to 13 times the possibility of moderate DTF events. This ratio escalates to 3 to 31
481 times for FTD events. Notably, severe FTD events are extremely rare, often occurring at 0% probability.
482 However, severe DTF events are notable, with probabilities ranging from 0% to 0.38%, and in some

483 instances, accounting for up to 13% of total DTF probability.
 484 The total probability of DTF events exceeds that of FTD events (Fig. 5a), and this holds true for mild,
 485 moderate, and severe intensity events (Fig. 6). The disparity between DTF and FTD events is not as
 486 pronounced in mild intensity events, but it becomes significant in moderate intensity events. The
 487 probabilities of moderate DTF range from 0.08% to 0.75%, whereas the probabilities of moderate FTD
 488 range from 0.04% to 0.42% (Fig. 6). The marked disparity in severe intensity events is even more
 489 pronounced by the extremely low probability of severe FTD.



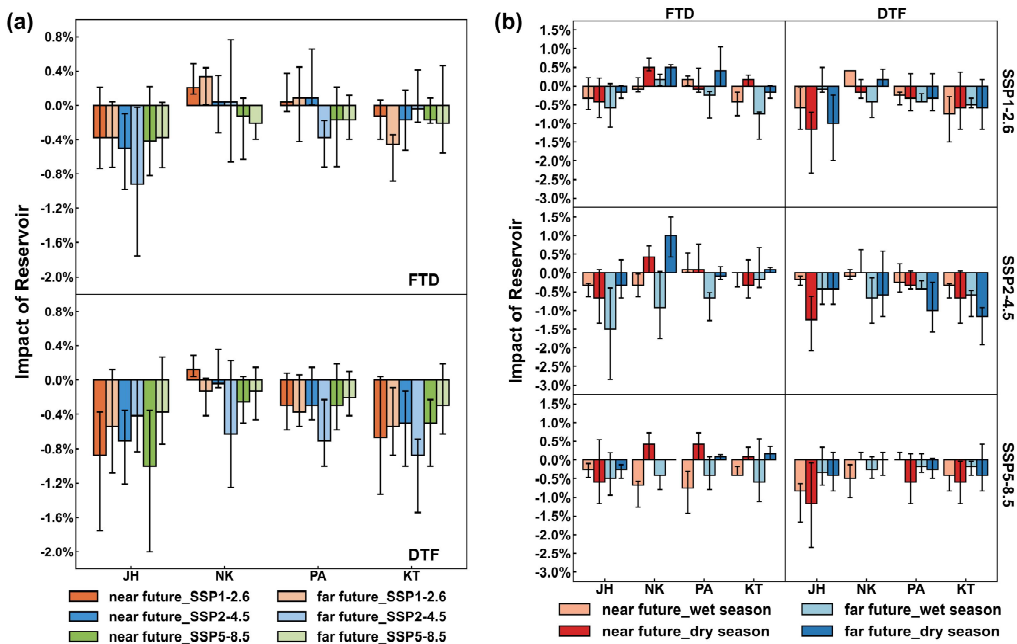
490
 491 **Figure 6: Annual probability of DFAA at different intensities under the natural scenario, averaged across**
 492 **five GCMs and their ranges in the near future (2021-2060) and far future (2061-2100) periods under three**
 493 **SSPs. Here, JH, NK, PA, and KT respectively denote JingHong, Nong Khai, Pakse, and Kratie stations.**

494 Mild DTF probabilities are projected to increase in the far future, while moderate and severe DTF
 495 probabilities are projected to decrease. Specifically, the probability of mild DTF rises to 1.1% to 2.4%
 496 in the far future, compared to 0.7% to 2.3% in the near future. The probabilities of moderate and severe
 497 DTF drop from an average of 0.42% and 0.19% in the near future to 0.38% and 0.12%, respectively, in
 498 the far future. However, the probabilities of FTD events across all three intensity levels remain
 499 relatively consistent between the near and far future.

500 3.4 Reservoirs' impacts on DFAA

501 Reservoirs exhibit extraordinary mitigation effects on DTF risk under the changing climate while
 502 showing weaker effects in FTD risk (Fig. 7a). Nonetheless, the higher probability of DTF compared to
 503 FTD (Fig. 5a) demonstrates that reservoirs contribute significantly to reducing overall DFAA risk.

504 Reservoirs adequately reduce or only slightly increase the future DTF probability (-0.13% to 1%,
 505 averaged across five GCMs. Throughout this section, a negative value indicates that reservoirs increase
 506 the probability of DFAA, while positive values indicate a reduction. In most scenarios, the reservoir
 507 plays a positive mitigating role across all GCMs (Fig. 7a). Reservoirs are expected to have better
 508 mitigation effects in the near future at JingHong station. As for Nong Khai and Pakse stations, the
 509 reduction effect of reservoirs on DTF is more pronounced in the far future under SSP1-2.6 and
 510 SSP2-4.5 scenarios, while in the near future under the SSP5-8.5 scenario. The effect conversely,
 511 exhibits greater strength under SSP1-2.6 and SSP5-8.5 scenarios in the near future, while it is stronger
 512 under the SSP2-4.5 scenario in the far future at Kratie station. These findings are consistent across both
 513 the average of the GCMs and their ranges.

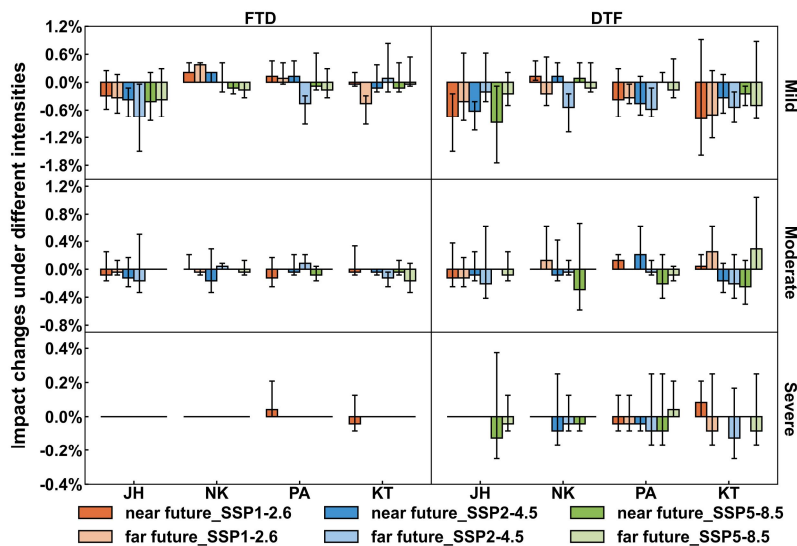


514
 515 **Figure 7: Reservoir impacts on DFAA during the near future (2021-2060) and the far future (2061-2100)**
 516 under three SSPs. Here, JH, NK, PA, and KT denote JingHong, Nong Khai, Pakse, and Kratie stations,
 517 respectively. (a) The annual reservoir impacts averaged across five GCMs and their ranges. (b) The
 518 seasonal reservoir impacts in wet and dry seasons averaged across five GCMs and their ranges.

519 Reservoirs are more effective in reducing FTD in the near future than in the far future at JingHong,
 520 Pakse, and Kratie, while the effect at Nong Khai is slightly less in the far future (Fig. 7b). Reservoirs
 521 are most effective under high emissions (SSP5-8.5), reducing FTD probability at all stations (0.13% to
 522 0.42%, GCM average). Under lower emissions (SSP1-2.6 and SSP2-4.5), mitigation is weaker (-0.33%
 523 to 0.38%, GCM average) at Nong Khai and Pakse, but notable at JingHong and Kratie, especially in

524 certain future periods. For example, under intermediate emissions (SSP2-4.5) in the far future at
 525 JingHong, reservoirs lower the average probability by over 0.9% and maximum by nearly 1.8%.
 526 Reservoirs reduce FTD more in the wet season (-0.17% to 1.5%, GCM average) than in the dry season
 527 (-1% to 0.67%), especially at Nong Khai, Pakse, and Kratie (Fig. 7b). Negative values mean a reservoir
 528 increases FTD probability. In the wet season, reduction is notable (-0.17% to 0.92%), but in the dry
 529 season, FTD probability increases (-1% to 0.33%). Seasonal differences in DTF mitigation are less
 530 pronounced. Reservoirs slightly better reduce DTF in the dry season (-0.17% to 1.25%) than in the wet
 531 season (-0.42% to 0.83%). Reservoirs mitigate DTF more effectively than FTD in both seasons,
 532 aligning with the annual DFAA.

533 Reservoirs effectively manage DFAA events, which are predominantly characterized by mild intensity.
 534 They decrease the probability of mild DTF by -0.1% to 0.9% (Fig. 8), whereas the probability of such
 535 events is 0.7% to 2.4% under the natural scenario (Fig. 6), indicating that reservoirs decrease their
 536 likelihood by -0.12 to 0.64 times. Reservoir reduces the probability of mild FTD by -0.4% to 0.8% (Fig.
 537 8). They increase the probability of mild FTD at the Nong Khai station under the SSP1-2.6 scenario.
 538 Since the probability of mild FTD is 0.6% to 1.8% under the natural scenario (Fig. 6), reservoir
 539 operation reduces their probability by -0.38 to 0.69 times.

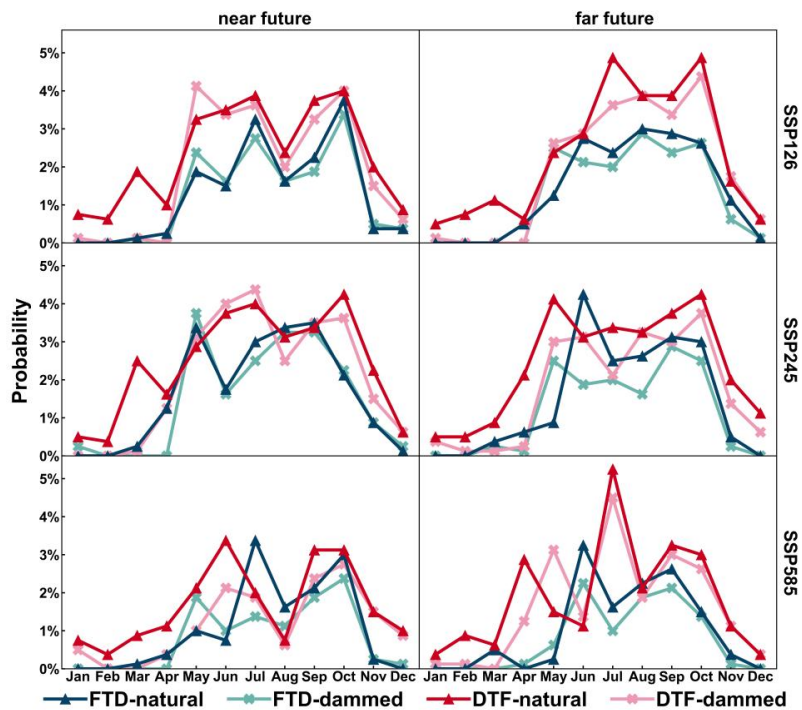


540
 541 **Figure 8: Reservoir impacts on DFAA under different intensities, averaged across five GCMs and their**
 542 **ranges in the near future (2021-2060) and far future (2061-2100) periods under three SSPs. Here, JH, NK,**
 543 **PA, and KT respectively denote JingHong, Nong Khai, Pakse, and Kratie stations.**

544 While the reservoir's mitigation effect on FTD events is less pronounced than on DTF events (Fig. 7), it
 545 demonstrates a commendable mitigation effect on moderate FTD, reducing their probability by -0.08%

546 to 0.17% (Fig. 8). This reduction represents -0.4 to 1 times the probability under the natural scenario.
 547 This ratio surpasses the reservoir's mitigation effect on moderate DTF, where the probability is reduced
 548 by -0.3% to 0.3% (Fig. 8), accounting for -0.70 to 1 times the natural probability. This highlights that
 549 the reservoir exerts a more significant mitigating force on high-intensity FTD events compared to
 550 high-frequency FTD events.

551 Reservoir exhibits notable mitigating effects for DTF events across all three intensity levels. However,
 552 their ability to alleviate moderate DTF is relatively weaker than that for mild DTF (Fig. 8), which
 553 differs from the characteristic of FTD events. This implies that reservoirs possess a stronger capability
 554 to manage high-frequency DTF events than higher-intensity events.



555
 556 **Figure 9: Monthly DFAA probability averaged over four mainstream hydrological stations (i.e., JingHong,
 557 Nong Khai, Pakse, and Kratie stations) under natural and dammed scenarios for three SSPs during the
 558 near future (2021-2060) and far future (2061-2100) periods. Please note that the probabilities shown in this
 559 figure are averaged over 5 GCMs.**

560 DFAA often shows several monthly peaks under the natural scenario. This means some months have a
 561 higher DFAA probability than their neighbors. The multiple peaks are clearer in DTF than in FTD (Fig.
 562 9). When averaging monthly DFAA over four mainstream hydrological stations, DTF shows three
 563 peaks under near-term SSP2-4.5 and far-term SSP5-8.5 scenarios, while FTD only shows two peaks in
 564 both cases. Reservoirs help regulate DFAA by lowering and reducing peaks, with a stronger peak

565 reduction effect anticipated in the near future for DTF (Fig. 9). In the far future, for FTD, especially
566 under SSP1-2.6 and SSP2-4.5, reservoirs still alleviate peaks, though less so in terms of reducing their
567 number. Reservoirs also lower DFAA probability during early and middle dry seasons (December to
568 April) for both near and far future futures, often 1% or less at most stations. Sometimes, such as the
569 SSP2-4.5 scenario in the near future, reservoirs actually increase the probability of DFAA in May. This
570 happens because helping during the dry season before May reduces the capacity of reservoirs for water
571 regulation in May, making it hard to control DFAA risks that month. Reservoirs also shorten DFAA's
572 monthly span. Instead of occurring throughout the year under the natural scenario, DFAA is to
573 concentrated from May to October under the dammed scenario (Fig. 9). This allows the LMR Basin to
574 focus DFAA policies and actions on those months. As a result, riparian states can combine resources
575 and coordinate their efforts more efficiently to manage and respond to DFAA and related hazards.

576 **4. Discussion**

577 **4.1 Different characteristics of DTF and FTD events**

578 The distinct characteristics of DTF and FTD events have been identified by previous research. Shi et al.
579 (2021) found that FTD events predominate in the Wei River Basin. Wang et al. (2023) projected that in
580 the Poyang Lake Basin, the temporal spread of DTF events will expand in the future, while that of FTD
581 events will constrict. Ren et al. (2023) found that under SSP1-2.6 and SSP2-4.5 scenarios, the
582 Huang-Huai-Hai River Basin will experience more DTF events, whereas under SSP3-7.0 and SSP5-8.5
583 scenarios, it will experience more FTD events. This study identifies differences between DTF and FTD
584 events as well, and further highlights the different characteristics of reservoirs' mitigating effects on
585 these events.

586 The average probability of DTF across all periods is 2.1% under the natural scenario, which is
587 significantly higher than the 1.4% average for FTD (Fig. 5a). The probability of DTF consistently
588 exceeds that of FTD under three different intensities (Fig. 6). Additionally, DTF probabilities show a
589 significant increase in both the near and far future, averaging 0.23%, which exceeds the increase in
590 FTD probabilities, averaging 0.13% (Fig. 5b).

591 Compared with FTD events, reservoirs more effectively control DTF probabilities, significantly
592 lowering DTF risk in both dry and wet seasons (Fig. 7). The reason is that the timing of DTF's water

593 regulation matches the way reservoirs operate. At the start of DTF, reservoirs typically hold water at the
594 storage corresponding to the normal water level, which equates to 0.8 times the maximum storage (Eq.
595 (20)). Hence, reservoirs possess sufficient storage capacity to mitigate the drought conditions. In
596 parallel, the water release during the initial phase of the DTF reduced the water level, thereby meeting
597 the storage needs for sudden floods that occur later in the DTF. As a result, even if DTF events are
598 frequent, reservoirs can manage them well. Reservoirs especially succeed in reducing mild DTF events
599 (Fig. 8). However, they control moderate DTF events less effectively. In intense DTF cases, the rules
600 for operating reservoirs are not enough. For example, if a severe drought at DTF's beginning exceeds
601 reservoir storage, they cannot effectively relieve the extreme drought and thus fail to control such DTF
602 events.

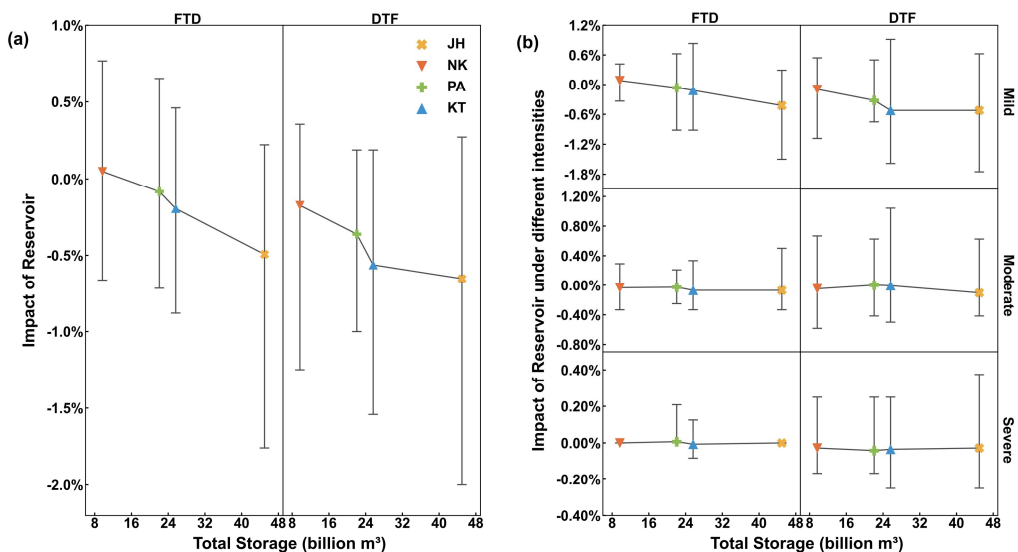
603 Although FTD is less likely than DTF, reservoirs control FTD less effectively, especially in the dry
604 season (Fig. 7). The problem is that when the FTD event occurs, reservoirs are generally maintained at
605 their target storage for the wet season. The storage corresponds to the flood control water level, which
606 is 1.2 times the minimum storage capacity (Eq. (19)). Consequently, reservoirs, while fully meeting
607 flood control requirements at the start of FTD, struggle to maintain sufficient water storage to satisfy
608 water supply demands for the subsequent drought stage. If FTD happens often, the reservoir's control
609 decreases further. While reservoirs do little for mild FTD, they noticeably reduce moderate FTD (Fig.
610 8). This means that, for rare but strong FTD events, reservoirs can help by storing water for later
611 droughts. However, if FTD is frequent, current reservoir operations do not help much. This difficulty in
612 regulation is what makes FTD a major challenge. It is encouraging, though, that FTD is expected to
613 become less common in most areas of the LMR Basin in the future (Fig. 5).

614 **4.2 The relationship between reservoirs' mitigation roles and their storage**

615 The reservoir systems provide enhanced mitigation efficiency against DFAA at JingHong and Kratie
616 compared to those at Nong Khai and Pakse (Fig. 7). Reservoir storage in the region above JingHong
617 and the Pakse to Kratie region is significantly larger than storage in the JingHong to Nong Khai and
618 Nong Khai to Pakse regions (Fig. 1c). Reservoirs' capacity to reduce total DFAA risk closely relates to
619 the total storage of mainstream and tributary reservoirs, consistently showing a positive correlation for
620 DTF and FTD events (Fig. 10a). These findings highlight reservoirs' multifaceted role in managing
621 flood prevention and drought resistance (Hecht et al., 2019; Hoang et al., 2019; Ly et al., 2023) while

622 also addressing sudden DFAA challenges. These results align with Feng et al.'s (2024) discovery that
 623 large reservoirs significantly reduce drought and flood risks and corroborate Ehsani et al.'s (2017)
 624 conclusion that increased dam dimensions can mitigate water resource vulnerability to climate
 625 uncertainties.

626 The positive correlation between total reservoir storage and the reduction of total DFAA risk indicates
 627 that basins with larger total storage are better equipped to resist DFAA events. However, this study
 628 examines only hydroelectric reservoirs in the LMR Basin and excludes other water storage facilities
 629 such as irrigation reservoirs. In the LMR Basin, total storage of irrigation reservoirs is considerable.
 630 According to the MRC, the Mekong Basin contains 1317 irrigation reservoirs, with total storage of
 631 about 17 billion m³ (MRC, 2018; LMC and MRC, 2023). This storage exceeds the total storage of
 632 reservoirs between JingHong and Nong Khai stations (around 9.7 billion m³). It is slightly lower than
 633 the storage between Nong Khai and Pakse stations (approximately 22.1 billion m³) (Figs. 1c and 10).
 634 Since reservoirs mitigate extreme hydrological events regardless of their primary function (Brunner,
 635 2021a; Ho and Ehret, 2025), even irrigation reservoirs can play a beneficial role in addressing DFAA
 636 events. Fully utilizing irrigation reservoirs and implementing coordinated operation of all reservoir
 637 types across the LMR Basin could effectively lower DFAA risks and enhance the basin's resistance to
 638 these events.



639

640 **Figure 10: The relationship between reservoirs' mitigation effects and their total storage. Symbol points**
 641 **denote the average values for each station under three SSP scenarios during the near future (2021-2060)**
 642 **and far future (2061-2100) periods, while error bars indicate the maximum and minimum values. Here, JH,**
 643 **NK, PA, and KT respectively denote JingHong, Nong Khai, Pakse, and Kratie stations. (a) The impact of**

644 reservoirs on the total probability of DFAA. (b) The impact of reservoirs on DFAA of different intensities.
645 Please note that, as Jinghong and Nong Khai stations are not expected to experience severe FTD in the
646 future, the relevant information has not been included in the figure.

647 Both mild DTF and mild FTD show a positive correlation with total reservoir storage, consistent with
648 total DFAA events (Fig. 10b). In contrast, moderate and severe DFAA events do not strongly correlate
649 with reservoir storage (Fig. 10b). This implies that for moderate to severe DFAA events, increasing
650 reservoir storage capacity does not enhance the reservoirs' control capabilities. Therefore, refining
651 reservoir operation rules presents a more appropriate strategy to strengthen control of moderate and
652 severe DFAA events in the LMR Basin.

653 **4.3 Limitations of reservoir regulation rules**

654 The reservoir operation rule SOP adopted in this study is a commonly used method. Previous studies
655 have widely employed this method (Wang et al., 2017a; Yun et al., 2020). The SOP rule is proven
656 appropriate for hydrological modeling in large-scale basins such as the LMR Basin. It is also effective
657 for extended simulation periods in future hydrological assessments (Wang et al., 2017b; Yun et al.,
658 2021a; Yun et al., 2021b).

659 This study further improved the standard SOP operation rules by adding the general case and
660 emergency case (Fig. 2). This scheduling approach manages reservoir operations using real-time inflow
661 data. It also considers the operational year of each reservoir. As a result, the reservoir module
662 developed in this study is robust and adaptable. It reflects reservoir scheduling scenarios with high
663 reliability.

664 Despite this, the study uses uniform operation rules for reservoirs of different storage scales within the
665 LMR Basin. It implements daily regulation for all reservoirs. The study does not use differentiated
666 regulation scales (daily, annual, or multi-annual) based on storage. It also does not consider unique
667 operation rules in different sub-basins. These simplifications may cause uncertainties in how reservoirs
668 mitigate effects. This is a limitation of the study.

669 **5. Conclusion**

670 This study adopts CMIP6 meteorological data, applying three SSP scenarios and five GCMs. It corrects
671 these data using the MBCn method. The study integrates the THREW distributed hydrological model

672 and the developed reservoir module. It describes DFAA through R-SDFAI, assessing mild, moderate,
673 and severe intensities. The study explores how reservoirs help reduce DFAA under the changing
674 climate in the LMR Basin. It examines three periods: history (1980-2014), near future (2021-2060),
675 and far future (2061-2100). The main findings are summarized below:

676 1. DFAA in the LMR Basin is dominated by DTF, with a mean probability of 2.1%. This is much
677 higher than the FTD probability of 1.4%. DTF remains higher than FTD at all intensity levels. The
678 future increase in DTF probability (average 0.23%) is also greater than the increase for FTD (average
679 0.13%). Mild-intensity DFAA events are most common. They account for 58% to 90% of future DTF
680 probability and 75% to 100% of FTD probability. Both DTF and FTD present higher DFAA risk during
681 the wet season than the dry season.

682 2. Reservoirs manage DTF probability well, cutting DTF risks in both dry and wet seasons. However,
683 they have less influence over FTD risks, especially during dry-season FTD events. Limited capacity to
684 control FTD risks is a challenge. Reservoirs do better at managing high-frequency DTF and
685 high-intensity FTD events. They also cut down multi-peak DFAA events and reduce their monthly
686 duration.

687 3. Reservoirs' ability to lower DFAA total risk is linked to their combined storage. Using large
688 irrigation reservoirs within the LMR Basin can help withstand mild DFAA risks and overall events. To
689 better handle moderate and severe DFAA events, reservoir operations need to be optimized.

690 This study gives new insights into how reservoirs help mitigate DFAA in the LMR Basin. It also aids
691 water management for riparian countries. DFAA remains a serious challenge. This shows the need for
692 LMR Basin countries to work together, build capacity against DFAA events, reduce climate change
693 effects, and support sustainable development.

694 **Author contribution**

695 **KZ:** Conceptualization; Data curation; Model development; Investigation; Methodology; Validation;
696 Visualization; Writing - original draft; Writing - review & editing. **ZZ:** Writing - review & editing. **FT:**
697 Conceptualization; Funding acquisition; Investigation; Methodology; Supervision; Writing - review &
698 editing.

699 **Competing interests**

700 At least one of the (co-)authors is a member of the editorial board of Hydrology and Earth System
701 Sciences.

702 **Data availability**

703 The hydrological data can be accessed and requested from the MRC Data Portal
704 (<https://portal.mrcmekong.org/home>, last access: October 2025). Information related to dams is
705 available on the Mekong Region Futures Institute (MERFI) website
706 (<https://www.merfi.org/mekong-region-dams-database>, last access: October 2025). The raw CMIP6
707 data without correction is available at (<https://esgf-node.llnl.gov/search/cmip6/>, last access: October
708 2025). The MBCn algorithm can be accessed and implemented through an R package, which is
709 available at (<https://CRAN.R-project.org/package=MBC>, last access: October 2025).

710 **Acknowledgment**

711 This research was funded by the National Natural Science Foundation of China (51961125204,
712 U2442201).

713 **Reference**

714 Adikari, Y. and Yoshitani, J.: Global Trends in Water-Related Disasters: An Insight for Policymakers,
715 International Centre for Water Hazard and Risk Management (ICHARM). The United Nations World
716 Water Development Report 3, Tsukuba, Japan, <https://unesdoc.unesco.org/ark:/48223/pf0000181793>
717 (last access: October 2025), 2009.

718 ADREM, SNSE, NDRC, IFRC and IRDR: 2023 Global Natural Disaster Assessment Report. Bejing,
719 <https://reliefweb.int/report/world/2023-global-natural-disaster-assessment-report> (last access: October
720 2025), 2024.

721 Arias, M., Piman, T., Lauri, H., Cochrane, T., Kummu, M.: Dams on Mekong tributaries as significant
722 contributors of hydrological alterations to the Tonle Sap Floodplain in Cambodia. Hydrol. Earth Syst.
723 Sci. 18, 5305-5315. <https://doi.org/10.5194/hess-18-5303-2014>, 2014.

724 Bai X., Zhao C., Tang Y., Zhang Z., Yang B. and Wang Z.: Identification, physical mechanisms and
725 impacts of drought–flood abrupt alternation: a review. Front. Earth Sci. 11:1203603,
726 <https://doi.org/10.3389/feart.2023.1203603>, 2023.

727 Brunner, M.: Reservoir regulation affects droughts and floods at local and regional scales. Environ. Res.
728 Lett. 16 (12). <https://doi.org/10.1088/1748-9326/ac36f6>, 2021.

729 Chen Z., Li X., Zhang X., et al.: Global drought-flood abrupt alternation: Spatio-temporal patterns,
730 drivers, and projections. The Innovation Geoscience 3:100113,
731 <https://doi.org/10.59717/j.xinn-geo.2024.100113>, 2025.

732 Cui, T., Li, Y., Yang, L., Nan, Y., Li, K., Tudaji, M., Tian, F.: Non-monotonic changes in Asian Water
733 Towers' streamflow at increasing warming levels. *Nature Communication*, 14(1), 1176,
734 <https://doi.org/10.1038/s41467-023-36804-6>, 2023.

735 Cannon, A.: Multivariate Bias Correction of Climate Model Output: Matching Marginal Distributions
736 and Intervariable Dependence Structure. *J. Clim.* 29, 7045–7064,
737 <https://doi.org/10.1175/JCLI-D-15-0679.1>, 2016

738 Cannon, A.: Multivariate quantile mapping bias correction: an N-dimensional probability density
739 function transform for climate model simulations of multiple variables. *Clim. Dyn.* 50, 31–49,
740 <https://doi.org/10.1007/s00382-017-3580-6>, 2018.

741 Dang, H. and Pokhrel, Y.: Evolution of river regimes in the Mekong River basin over 8 decades and the
742 role of dams in recent hydrological extremes, *Hydrol. Earth Syst. Sci.*, 28, 3347–3365,
743 <https://doi.org/10.5194/hess-28-3347-2024>, 2024.

744 Do, P., Tian, F., Zhu, T., Zohidov, B., Ni, G., Lu, H., Liu, H.: Exploring synergies in the
745 water-food-energy nexus by using an integrated hydro-economic optimization model for the
746 Lancang-Mekong River basin. *Sci. Total Environ.* 728, 137996,
747 <https://doi.org/10.1016/j.scitotenv.2020.137996>, 2020.

748 Dong, Z., Liu, H., Baiyinbaoligao, Hu, H., Khan, M., Wen, J., Chen, L., Tian, F.: Future projection of
749 seasonal drought characteristics using CMIP6 in the Lancang-Mekong River Basin. *J. Hydrol.* 610,
750 <https://doi.org/10.1016/j.jhydrol.2022.127815>, 2022.

751 Ehsani, N., Vörösmarty, C., Fekete, B., Stakhiv, E.: Reservoir operations under climate change: storage
752 capacity options to mitigate risk. *J. Hydrol.* 555, 435–446.
753 <https://doi.org/10.1016/j.jhydrol.2017.09.008>, 2017.

754 Eyring, V., Bony, S., Meehl, G., Senior, C., Stevens, B., Stouffer, R., Taylor, K.: Overview of the
755 Coupled Model Intercomparison Project Phase 6 (CMIP6) experimental design and organization,
756 *Geosci. Model Dev.*, 9, 1937–1958, <https://doi.org/10.5194/gmd-9-1937-2016>, 2016.

757 Feng, J., Qin, T., Yan, D., Lv, X., Yan, D., Zhang, X., Li, W.: The role of large reservoirs in drought and
758 flood disaster risk mitigation: a case of the Yellow River Basin. *Sci. Total Environ.* 949, 175255.
759 <https://doi.org/10.1016/j.scitotenv.2024.175255>, 2024.

760 Gidden, M., Riahi, K., Smith, S., Fujimori, S., Luderer, G., Kriegler, E., van Vuuren, D., van den Berg,
761 M., Feng, L., Klein, D., Calvin, K., Doelman, J., Frank, S., Fricko, O., Harmsen, M., Hasegawa, T.,
762 Havlik, P., Hilaire, J., Hoesly, R., Horing, J., Popp, A., Stehfest, E., Takahashi, K.: Global emissions
763 pathways under different socioeconomic scenarios for use in CMIP6: a dataset of harmonized
764 emissions trajectories through the end of the century, *Geosci. Model Dev.*, 12, 1443–1475,
765 <https://doi.org/10.5194/gmd-12-1443-2019>, 2019.

766 Gunawardana, S., Shrestha, S., Mohanasundaram, S., Salin, K., Piman, T.: Multiple drivers of
767 hydrological alteration in the transboundary Srepok River Basin of the Lower Mekong Region. *J.*
768 *Environ. Manage.* 278, 111524, <https://doi.org/10.1016/j.jenvman.2020.111524>, 2021.

769 He D.: Analysis on the hydrological characteristics of Lancang-Meigong River. *Yunnan Geographic*
770 *Environment Research*, 1, 58-74 (in Chinese), 1995.

771 Hecht, J., Lacombe, G., Arias, M., Dang, T., Piman, T.: Hydropower dams of the Mekong River basin:
772 A review of their hydrological impacts. *J. Hydrol.* 568, 285–300,
773 <https://doi.org/10.1016/j.jhydrol.2018.10.045>, 2019.

774 Ho, S. and Ehret, U.: Is drought protection possible without compromising flood protection?
775 Estimating the potential dual-use benefit of small flood reservoirs in southern Germany, *Hydrol. Earth*

776 Syst. Sci., 29, 2785–2810, <https://doi.org/10.5194/hess-29-2785-2025>, 2025.

777 Hoang, L., van Vliet, M., Kummu, M., Lauri, H., Koponen, J., Supit, I., Leemans, R., Kabat, P.,
778 Ludwig, F.: The Mekong's future flows under multiple drivers: How climate change, hydropower
779 developments and irrigation expansions drive hydrological changes. Sci. Tot. Environ.,
780 <https://doi.org/10.1016/j.scitotenv.2018.08.160>, 2019.

781 IPCC: Sections. In: Climate Change 2023: Synthesis Report. Contribution of Working Groups I, II and
782 III to the Sixth Assessment Report of the Intergovernmental Panel on Climate Change [Core Writing
783 Team, H. Lee and J. Romero (eds.)]. IPCC, Geneva, Switzerland, pp. 35–115,
784 <https://doi.org/10.59327/IPCC/AR6-9789291691647>, 2023.

785 IPCC Working Group I: Contribution to the Sixth Assessment Report of the Intergovernmental Panel
786 on Climate Change. Climate Change; The Physical Science Basis. TS-93,
787 <https://www.ipcc.ch/report/ar6/syr/> (last access: October 2025), 2021.

788 Khadka, D., Babel, M., Kamalamma, A.: Assessing the Impact of Climate and Land-Use Changes on
789 the Hydrologic Cycle Using the SWAT Model in the Mun River Basin in Northeast Thailand. Water, 15,
790 3672, <https://doi.org/10.3390/w15203672>, 2023.

791 Kingston, D., Thompson, J., Kite, G.: Uncertainty in climate change projections of discharge for the
792 Mekong River Basin, Hydrol. Earth Syst. Sci., 15, 1459–1471,
793 <https://doi.org/10.5194/hess-15-1459-2011>, 2011.

794 Lancang-Mekong Water Resources Cooperation Center (LMC) and Mekong River Commission (MRC):
795 Technical Report - Phase 1 of the Joint Study on the Changing Patterns of Hydrological Conditions of
796 the Lancang-Mekong River Basin and Adaptation Strategies. Beijing: LMC Water Center or Vientiane:
797 MRC Secretariat, http://www.lmcwater.org.cn/cooperative_achievements/collaborative_projects/ (last
798 access: October 2025), <https://www.mrcmekong.org/publication/> (last access: October 2025), 2023.

799 Lange, S.: Trend-preserving bias adjustment and statistical downscaling with ISIMIP3BASD (v1.0),
800 Geoscientific Model Development, 12, 3055–3070, <https://doi.org/10.5194/gmd-12-3055-2019>, 2019.

801 Lange, S.: ISIMIP3BASD v2.5.0, <https://doi.org/10.5281/zenodo.4686991>, 2021.

802 Lauri, H., de Moel, H., Ward, P., Räsänen, T., Keskinen, M., Kummu, M.: Future changes in Mekong
803 River hydrology: impact of climate change and reservoir operation on discharge, Hydrol. Earth Syst.
804 Sci., 16, 4603–4619, <https://doi.org/10.5194/hess-16-4603-2012>, 2012.

805 Lei, X., Song, X., Guo, H., Ma, R., Song, S.: Analysis on spatio-temporal evolution characteristics of
806 short-cycle drought-flood sudden alteration and potential driving factors in the north-south transitional
807 zone of China. Journal of Natural Disasters. 31(4), 31–43 (in Chinese),
808 <https://doi.org/10.13577/j.jnd.2022.0403>, 2022.

809 Li, Y., Lu, H., Yang, K., Wang, W., Tang, Q., Khem, S., Yang, F., Huang, Y.: Meteorological and
810 hydrological droughts in Mekong River Basin and surrounding areas under climate change, J. Hydrol.:
811 Reg. Stud. 36, 100873, <https://doi.org/10.1016/j.ejrh.2021.100873>, 2021.

812 Liu, H., Yang, Z., Xu, F., Zhang, X., Baiyin, B., Mu, X., Hu, H.: Drought in Lancang-Mekong River
813 Basin and the impact of upstream reservoirs. J. China Inst. Water Resour. Hydropower Res. 6, 479–485
814 (in Chinese), <https://doi.org/10.13244/j.cnki.jiwhr.20200058>, 2020.

815 Lu, Y., Tian, F., Guo, L., Borzi, I., Patil, R., Wei, J., Liu, D., Wei, Y., Yu, D. J., Sivapalan, M.:
816 Socio-hydrologic modeling of the dynamics of cooperation in the transboundary Lancang–Mekong
817 River, Hydrol. Earth Syst. Sci., 25, 1883–1903, <https://doi.org/10.5194/hess-25-1883-2021>, 2021.

818 Lu, X., Li, S., Kummu, M., Padawangi, R., Wang, J.: Observed changes in the water flow at Chiang
819 Saen in the lower Mekong: impacts of Chinese dams? Quatern. Int.,

820 <https://doi.org/10.1016/j.quaint.2014.02.006>, 2014.

821 Luo, X., Luo, X., Ji, X., Ming, W., Wang, L., Xiao, X., Xu, J., Liu, Y., Li, Y.: Meteorological and
822 hydrological droughts in the Lancang-Mekong River Basin: spatiotemporal patterns and propagation.
823 Atmospheric Research 293, 106913. <https://doi.org/10.1016/j.atmosres.2023.106913>, 2023.

824 Ly, S., Sayama, T., Try, S.: Integrated impact assessment of climate change and hydropower operation
825 on streamflow and inundation in the lower Mekong Basin. Prog Earth Planet Sci 10, 55,
826 <https://doi.org/10.1186/s40645-023-00586-8>, 2023.

827 Mekong Region Futures Institute (MERFI): Dataset on the Dams of the Greater Mekong. Bangkok,
828 Mekong Region Futures Institute, <https://www.merfi.org/mekong-region-dams-database> (last access:
829 October 2025), 2024.

830 Mishra, V., Bhatia, U., Tiwari, A.: Bias-corrected climate projections for South Asia from Coupled
831 Model Intercomparison Project-6. Sci Data 7, 338, <https://doi.org/10.1038/s41597-020-00681-1>, 2020.

832 Morovati, K., Tian, F., Kummu, M., Shi, L., Tudaji, M., Nakhaei, P., Olivares, M.: Contributions from
833 climate variation and human activities to flow regime change of Tonle Sap Lake from 2001 to 2020.
834 Journal of Hydrology, 616, 128800, <https://doi.org/10.1016/j.jhydrol.2022.128800>, 2023.

835 Morovati, K., Tian, F., Pokhrel, Y., Someth, P., Shi, L., Zhang, K., Ly, S.: Fishery and agriculture
836 amidst human activities and climate change in the Mekong River: A review of gaps in data and
837 effective approaches towards sustainable development, J. Hydrol., 132043,
838 <https://doi.org/10.1016/j.jhydrol.2024.132043>, 2024.

839 Morris, G. and Fan, J.: Reservoir sedimentation handbook: Design and management of dams,
840 reservoirs, and watersheds for sustainable use. New York, NY: McGraw-Hill, 1998.

841 Mou, L., Tian, F., Hu, H., Sivapalan, M.: Extension of the Representative Elementary Watershed
842 approach for cold regions: constitutive relationships and an application, Hydrol. Earth Syst. Sci., 12,
843 565–585, <https://doi.org/10.5194/hess-12-565-2008>, 2008.

844 MRC: Assessment of Basin-Wide Development Scenarios—Main Report, Mekong River Commission,
845 <https://reliefweb.int/report/lao-peoples-democratic-republic/assessment-basin-wide-development-scena>
846 <rios-main-report> (last access: October 2025), 2010.

847 MRC: Irrigation Database Improvement for the Lower Mekong Basin. Vientiane, Lao PDR,
848 <https://www.mrcmekong.org/publications/irrigation-database-improvement-for-the-lower-mekong-river>
849 [-basin/#:~:text=It%20reviews%20the%20current%20situation%20of%20irrigation%20in,%28LMB%2](#)
850 [9%20and%20provides%20recommendations%20for%20further%20database%20impro](#) (last access:
851 October 2025), 2018.

852 MRC: State of the Basin Report 2018,
853 <https://www.mrcmekong.org/publications/state-of-the-basin-report-2018-2/> (last access: October 2025),
854 2019.

855 MRC: Annual Mekong hydrology, flood and drought report 2019: Drought in the Lower Mekong River
856 Basin. Vientiane: MRC Secretariat,
857 <https://www.mrcmekong.org/publications/annual-mekong-hydrology-flood-and-drought-report-2019-dr>
858 [ought-in-the-lower-mekong-basin/](#) (last access: October 2025), 2020.

859 Nan, Y., Tian, L., He, Z., Tian, F., Shao, L.: The value of water isotope data on improving process
860 understanding in a glacierized catchment on the Tibetan Plateau, Hydrol. Earth Syst. Sci., 25,
861 3653–3673, <https://doi.org/10.5194/hess-25-3653-2021>, 2021.

862 Räsänen, T., Koponen, J., Lauri, H., Kummu, M.: Downstream Hydrological Impacts of Hydropower
863 Development in the Upper Mekong Basin. Water Resour Manage 26, 3495–3513.

864 <https://doi.org/10.1007/s11269-012-0087-0>, 2012.

865 Ren, J., Wang, W., Wei, J., Li, H., Li, X., Liu, G., Chen, Y., Ye, S.: Evolution and prediction of
866 drought-flood abrupt alternation events in Huang-Huai-Hai River Basin, China. *Sci. Total Environ.* 869,
867 <https://doi.org/10.1016/j.scitotenv.2023.161707>, 2023.

868 Sabo, J., Puhi, A., Holtgrieve, G., Elliott, V., Arias, M., Ngor, B., Räsänen, T., Nam, S.: Designing river
869 flows to improve food security futures in the lower Mekong Basin. *Science* 358 (6368).
870 <https://doi.org/10.1126/science.aa01053>, 2017.

871 Schmitt, R., Bizzi, S., Castelletti, A., Kondolf, G.: Improved trade-offs of hydropower and sand
872 connectivity by strategic dam planning in the Mekong. *Nat Sustain* 1, 96–104,
873 <https://doi.org/10.1038/s41893-018-0022-3>, 2018.

874 Shan, L., Zhang, L., Song, J., Zhang, Y., She, D., Xia, J.: Characteristics of dry-wet abrupt alternation
875 events in the middle and lower reaches of the Yangtze River Basin and the relationship with ENSO.
876 *Acta Geographica Sinica*, 73(1): 25–40 (in Chinese), <https://doi.org/10.11821/dlxb201801003>, 2018.

877 Shi, W., Huang, S., Liu, D., Huang, Q., Han, Z., Leng, G., Wang, H., Hao, L., Li, P., Wei, X.:
878 Drought-flood abrupt alternation dynamics and their potential driving forces in a changing environment.
879 *J. Hydrol.* 597, 126179, <https://doi.org/10.1016/j.jhydrol.2021.126179>, 2021.

880 Sridhar, V., Kang, H., Ali, S.: Human-Induced Alterations to Land Use and Climate and Their
881 Responses for Hydrology and Water Management in the Mekong River Basin. *Water*, 11, 1307,
882 <https://doi.org/10.3390/w11061307>, 2019.

883 Song, X., Lei, X., Ma, R., Hou, J., Liu, W.: Spatiotemporal variation and multivariate controls of
884 short-cycle drought–flood abrupt alteration: A case in the Qinling-Daba Mountains of China.
885 *International Journal of Climatology*, 43(10), 4756–4769, <https://doi.org/10.1002/joc.8115>, 2023.

886 Sun, P., Zou, Y., Yao, R., Ma, Z., Bian, Y., Ge, C., Lv, Y.: Compound and successive events of extreme
887 precipitation and extreme runoff under heatwaves based on CMIP6 models. *Science of the Total
888 Environment*, 878, 162980, <https://doi.org/10.1016/j.scitotenv.2023.16298>, 2023.

889 Tellman, B., Sullivan, J.A., Kuhn, C. et al.: Satellite imaging reveals increased proportion of population
890 exposed to floods. *Nature* 596, 80–86, <https://doi.org/10.1038/s41586-021-03695-w>, 2021.

891 Tennant, D.: Instream flow regimens for fish, wildlife, recreation and related environmental resources.
892 *FISHERIES*, 1(4), 6–10, [https://doi.org/10.1577/1548-8446\(1976\)001<0006:IFRFFW>2.0.CO;2](https://doi.org/10.1577/1548-8446(1976)001<0006:IFRFFW>2.0.CO;2) 1976.

893 Thompson, J., Green, A., Kingston, D.: Potential evapotranspiration-related uncertainty in climate
894 change impacts on river flow: An assessment for the Mekong River basin. *Journal of Hydrology*, 510,
895 259–279. <https://doi.org/10.1016/j.jhydrol.2013.12.010>, 2014.

896 Tian, F., Liu, H., Hou, S., Li, K., Lu, H., Ni, G., Mu, X., Baiyinbaoligao: Drought characteristics of the
897 Lancang-Mekong Basin and the role of reservoir regulation on streamflow. *The international journal of
898 hydropower&dams*, 5, 81-89,
899 <http://www.thuwatert.org/admin/tp/Report-on-Lancang-Mekong-Drought-and-Reservoir-Regulation.pdf>
900 (last access: October 2025), 2020.

901 Tian, F., Hu, H., Lei, Z., Sivapalan, M.: Extension of the Representative Elementary Watershed
902 approach for cold regions via explicit treatment of energy related processes, *Hydrol. Earth Syst. Sci.*,
903 10, 619–644, <https://doi.org/10.5194/hess-10-619-2006>, 2006.

904 Tian, F., Li, H., Sivapalan, M.: Model diagnostic analysis of seasonal switching of runoff generation
905 mechanisms in the Blue River basin, Oklahoma. *J. Hydrol.* 418 (419), 136–149,
906 <https://doi.org/10.1016/j.jhydrol.2010.03.011>, 2012.

907 Van Pelt, S., Kabat, P., ter Maat, H., van den Hurk, B., Weerts, A.: Discharge simulations performed

908 with a hydrological model using bias corrected regional climate model input, *Hydrol. Earth Syst. Sci.*,
909 13, 2387–2397, <https://doi.org/10.5194/hess-13-2387-2009>, 2009.

910 Wang, A., Miao, Y., Kong, X., Wu, H.: Future changes in global runoff and runoff coefficient from
911 CMIP6 multi-model simulation under SSP1-2.6 and SSP5-8.5 scenarios. *Earth's Future*, 10(12),
912 e2022EF002910. <https://doi.org/10.1029/2022EF002910>, 2022.

913 Wang, C., Leisz, S., Li, L., Shi, X., Mao, J., Zheng, Y., Chen, A.: Historical and projected future runoff
914 over the Mekong River basin, *Earth Syst. Dynam.*, 15, 75–90, <https://doi.org/10.5194/esd-15-75-2024>,
915 2024.

916 Wang, R., Li, X., Zhang, Q., Cheng, J., Li, J., Zhang, D., Liu, Y.: Projection of drought-flood abrupt
917 alternation in a humid subtropical region under changing climate. *J. Hydrol.* 624, 129875,
918 <https://doi.org/10.1016/j.jhydrol.2023.129875>, 2023.

919 Wang, S., Zhang, L., She, D., Wang, G., Zhang, Q.: Future projections of flooding characteristics in the
920 Lancang-Mekong River Basin under climate change. *J. Hydrol.* 602,
921 <https://doi.org/10.1016/j.jhydrol.2021.126778>, 2021.

922 Wang, W., Li, H. Y., Leung, L. R., Yigzaw, W., Zhao, J., Lu, H., Deng, Z., Demisie, Y., Blöschl, G.:
923 Nonlinear filtering effects of reservoirs on flood frequency curves at the regional scale, *Water Resour.
924 Res.*, 53, 8277–8292, <https://doi.org/10.1002/2017WR020871,2017>, 2017a.

925 Wang, W., Lu, H., Leung, L. R., Li, H., Zhao, J., Tian, F., Yang, K., Sothea, K.: Dam construction in
926 Lancang-Mekong River Basin could mitigate future flood risk from warming-induced intensified
927 rainfall. *Geophysical Research Letters*, 44, 10,378–10,386, <https://doi.org/10.1002/2017GL075037>,
928 2017b.

929 Wu, Z., Li, J., He, J., Jiang, Z.: Large-scale atmospheric singularities and summer long-cycle
930 droughts–floods abrupt alternation in the middle and lower reaches of the Yangtze River. *Chinese
931 Science Bulletin*, 51(16), 2027–2034, <https://doi.org/10.1007/s11434-006-2060-x>, 2006.

932 Williams, J.: The hydropower myth. *Environ. Sci. Pollut. R.*,
933 <https://doi.org/10.1007/s11356-019-04657-6>, 2019.

934 Xiong, J. and Yang, Y.: Climate Change and Hydrological Extremes. *Curr Clim Change Rep* 11, 1,
935 <https://doi.org/10.1007/s40641-024-00198-4>, 2025.

936 Yang, P., Zhang, S., Xia, J., Zhan, C., Cai, W., Wang, W., Luo, X., Chen, N., Li, J.: Analysis of drought
937 and flood alternation and its driving factors in the Yangtze River Basin under climate change. *J.
938 ATMOS. RES.* 270, 106087, <https://doi.org/10.1016/j.atmosres.2022.106087>, 2022.

939 Yang, Y., Weng, B., Bi, W., Xu, T., Yan, D., Ma, J.: Climate Change Impacts on Drought-Flood Abrupt
940 Alternation and Water Quality in the Hetao Area, China. *Water*, 11, 652,
941 <https://doi.org/10.3390/w11040652>, 2019.

942 Yuan, X., Wang, J., He, D., Lu, Y., Sun, J., Li, Y., Guo, Z., Zhang, K., Li, F.: Influence of cascade
943 reservoir operation in the upper Mekong River on the general hydrological regime: a combined
944 data-driven modeling approach. *J. Environ. Manag.* 324, 116339,
945 <https://doi.org/10.1016/j.jenvman.2022.116339>, 2022.

946 Yun, X., Tang, Q., Wang, J., Liu, X., Zhang, Y., Lu, H., Wang, Y., Zhang, L., Chen, D.: Impacts of
947 climate change and reservoir operation on streamflow and flood characteristics in the Lancang-Mekong
948 River Basin. *J. Hydrol.* 590, 125472, <https://doi.org/10.1016/j.jhydrol.2020.125472>, 2020.

949 Yun, X., Tang, Q., Li, J., Lu, H., Zhang, L., Chen, D.: Can reservoir regulation mitigate future climate
950 change induced hydrological extremes in the Lancang-Mekong River Basin? *Sci. Total Environ.* 785,
951 <https://doi.org/10.1016/j.scitotenv.2021.147322>, 2021a.

952 Yun, X., Tang, Q., Sun, S., Wang, J.: Reducing climate change induced flood at the cost of hydropower
953 in the Lancang-Mekong River Basin. *Geophysical Research Letters*, 48, e2021GL094243,
954 <https://doi.org/10.1029/2021GL094243>, 2021b.

955 Zhang, K., Morovati, K., Tian, F., Yu, L., Liu, B., Olivares, M.: Regional contributions of climate
956 change and human activities to altered flow of the Lancang-Mekong river. *J. Hydrol.: Reg. Stud.* 50,
957 101535, <https://doi.org/10.1016/j.ejrh.2023.101535>, 2023.

958 Zhang, S., Zhang, J., Min, J., Zhang, Z., Zhuang, J., Lin, J.: Drought–flood abrupt alternation based on
959 runoff in the Huaihe River Basin during rainy season. *Journal of Lake Sciences*, 24(5), 679–686 (in
960 Chinese), <https://doi.org/10.18307/2012.0506>, 2012.

961 Zhang, Z., Yuan, Y., Shen, D., Fan, H.: Identification of drought-flood Abrupt alternation in tobacco
962 growth period in Xingren county under climate change in China. *Appl. Ecol. Environ. Res.* 17,
963 12259–12269, https://doi.org/10.15666/aeer/1705_1225912269, 2019.

964 Zhao, D., Deng, S., Zhang, J.: Spatiotemporal characteristics of dry-wet abrupt alternation events in
965 China during 1960–2018. *International Journal of Climatology*, 42(16), 9612–9625,
966 <https://doi.org/10.1002/joc.7850>, 2022.